FOI-R--1243--SE
June 2004
ISSN 1650-1942
Scientific report

Karin Åhlund

Investigation of the NREL NASA/Ames Wind Turbine Aerodynamics Database

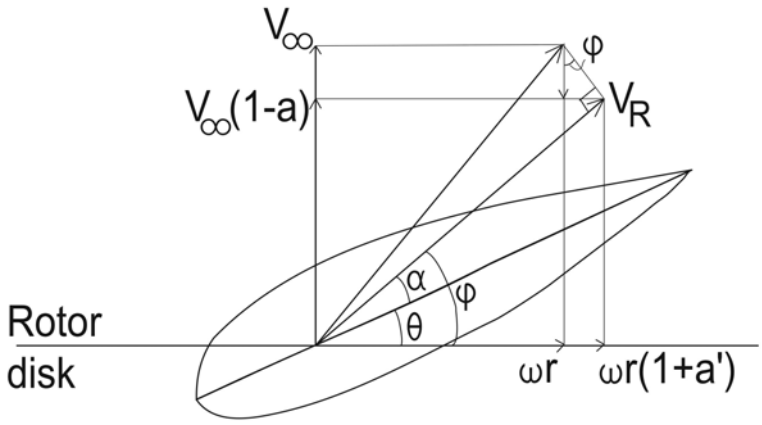

SWEDISH DEFENCE RESEARCH AGENCY
Aeronautics, FFA
SE-172 90 Stockholm

FOI-R--1243--SE
June 2004
ISSN 1650-1942
Scientific report

Karin Åhlund

Investigation of the NREL NASA/Ames Wind Turbine Aerodynamics Database

Issuing organization	Report number, ISRN	Report type
FOI – Swedish Defence Research Agency Aeronautics, FFA SE-172 90 Stockholm Sweden	FOI-R--1243--SE	Scientific Report
	Research area code 9. Civilian Applications Including Environmental	
	Month year June 2004	**Project no.** B827404
	Energimyndigheten 3. Aeronautical Research	
	Sub area code 91 Civil Applications	

Author/s (editor/s)	Project manager
Karin Åhlund	Björn Montgomerie
	Approved by Sven-Erik Thor
	Sponsoring agency Energimyndigheten
	Scientifically and technically responsible Björn Montgomerie

Report title
Investigation of the NREL NASA/Ames Wind Turbine Aerodynamics Database

Abstract

The original purpose of the project was to compare two-dimensional and three-dimensional behaviour of aerodynamic coefficients on wind turbines. Because of missing information in the database, the angle of attack distribution (AD) must first be calculated. The probes that were attached to the leading edge on one of the two blades were expected to lead to the AD. This was shown to be a difficult task. Three different attempts were made to calculate the AD. Since low angles of attack follow two-dimensional patterns, the AD could be calculated. The interesting area at high angles of attack, where the three-dimensional effects are strong, could not be evaluated.

For all similar experiments, the velocity of the air that passes through the turbine must be measured. Then the AD along a blade can easily be calculated.

Keywords
wind power, aerodynamics, wind tunnel, NREL, NASA

Further bibliographic information	Language English
ISSN 1650-1942	**Pages** 57 p.
	Price acc. to pricelist

Utgivare Totalförsvarets Forskningsinstitut - FOI Flygteknik FFA 172 90 Stockholm	**Rapportnummer, ISRN** FOI-R--1243--SE	**Klassificering** Vetenskaplig rapport
	Forskningsområde 9. Civila tillämpningar inklusive miljöfrågor	
	Månad, år Juni 2004	**Projektnummer** B827404
	Verksamhetsgren 3. Flygteknisk forskning	
	Delområde 91 Övriga civila tillämpningar	
Författare/redaktör Karin Åhlund	**Projektledare** Björn Montgomerie	
	Godkänd av Sven-Erik Thor	
	Uppdragsgivare/kundbeteckning Energimyndigheten	
	Tekniskt och/eller vetenskapligt ansvarig Björn Montgomerie	

Rapportens titel (i översättning)

Undersökning av NRELs NASA/Ames aerodynamiska vindturbindatabas

Sammanfattning

Det ursprungliga syftet med projektet var att undersöka skillnaderna mellan tvådimensionella och tredimensionella beteenden hos aerodynamiska koefficienter på vindturbinblad. Anfallsvinkelfördelningen (AD) måste då först beräknas, eftersom dessa data inte finns i databasen. Förhoppningarna ställdes till de trycksonder som var fästa i framkanten på ett av de två bladen. Tre olika försök att räkna ut AD gjordes. Vid låga anfallsvinklar råder tvådimensionella mönster och anfallsvinklarna kunde beräknas. Det intressanta området vid höga anfallsvinklar, med starka tredimensionella effekter, kunde inte utvärderas.

Slutsatsen är att för alla försök av samma typ måste hastigheten mätas för den luft som går genom rotorn varefter AD längs ett blad enkelt kan beräknas.

Nyckelord

Vindkraft, aerodynamik, vindtunnel, NREL, NASA

Övriga bibliografiska uppgifter	**Språk** Engelska
ISSN 1650-1942	**Antal sidor:** 57 s.
Distribution enligt missiv	**Pris: Enligt prislista**

Acknowledgements

This report is the thesis for my aeronautical engineering degree at the Mälardalen Högskola.

Many thanks go to my supervisor Björn Montgomerie at the Swedish Defence Research Agency, FOI, for all help during my time at FOI and for being such a good teacher and friend.

CONTENTS

Notation

a – axial induction factor
a' – angular induction factor
B – number of blades
c – chord length
C_D – drag coefficient
C_{Df} – friction drag coefficient
C_L – lift coefficient
$C_{L,inv}$ – lift coefficient for inviscid flow
$C_{L,2D}$ – measured lift coefficient from 2D tests
$C_{L,3D}$ – calculated lift coefficient in 3D
C_M – moment coefficient
C_N – normal force coefficient
C_P – power coefficient
C_T – tangential force coefficient
C_{Th} – thrust coefficient
f – multiplication correction factor in Snel's formula.
F_{tot} – Prandtl's total correction factor
F_P – Prandtl's general correction factor
P – shaft power
P_{max} – maximum shaft power
Q – torque
R – blade radius
r – radial coordinate of blade element
r_{HUB} – radius from center of hub to 8.45% of blade radius
dr – radial extent of blade element
RPM – revolutions per minute
s – distance from leading edge to the lifting line
T – thrust force
U – velocity at the turbine
V_∞ – free stream velocity
V – reduced velocity due to the turbine
V_2 – velocity after the turbine
V_D – resulting velocity at the probe head
V_R – resulting velocity
w – induced velocity
w_{B2} –induced velocity from the other blade
w_x – x-component of the induced velocity from the body
w_y – y-component of the induced velocity from the body
w_{tot} – induced velocity from the body
α – angle of attack
Φ, φ – relative flow angle
λx – equals $\omega r/V_\infty$
φ_A,φ_B – angles used in Biot-Savart's law
θ – blade angle = blade pitch angle + local twist angle
ρ – air density
ω – induced rotational angular velocity
ξ – LFA – Local flow angle
Γ – circulation
Π – coning angle

Ω – turbine angular velocity

Subscripts
1 – value at the probe head
2 – value at the blade
ber – calculated value

1 Background

The present state of the art in aerodynamic methods, for external forcing of wind turbine blades, relies on steady theory with additions for dynamic events. With phenomena like the Himmelskamp effect (section 1.7) where C_L reaches values greater than 3, it is shown that there are some dynamic events not included in the steady theories. This text reports an investigation of aerodynamic measurements on a ten meter diameter wind turbine with focus on steady aerodynamics. The purpose was to find a connection between two-dimensional and tree-dimensional effects. In order to do that, the angle of attack first had to be found due to lacking information from the NREL NASA/Ames database. For perspective, however, the first part of the report deals with some basics even including dynamic effects.

1.1 Basic BEM (Blade Element Momentum)

For calculating forces either computational fluid dynamics (CFD) or so called engineering methods can be used. CFD methods are very time consuming in the computer while the engineering methods are rapid. CFD replace the integrals of the partial derivatives in basic equations with discretized algebraic forms, which in turn are solved to obtain the flow field values at discrete points in time and/or space. Usually Navier-Stokes equations are used (see reference 1). CFD can take up to a week for solving large problems. The engineering methods only need a few seconds. In general calculations of wind turbine aerodynamics, especially in the context of aeroelastic simulations, engineering methods represent the only choice.

The BEM calculation method is based on a combination of blade element and momentum theory (see reference 8). The blade length is divided into small elements for which two-dimensional airfoil theory is applied. When strong three-dimensional effects occur the result will not be accurate. Dynamic inflow is a strong contributor to this problem, the ground boundary layer affects the inflow to the turbine, as do yawed turbines and gusts (see references 16 and 17). BEM is therefore used with certain correction factors, depending on how it is applied.

For the annular ring and corresponding control volume generated by each blade element (see figure 1), momentum theory is applied accordingly.

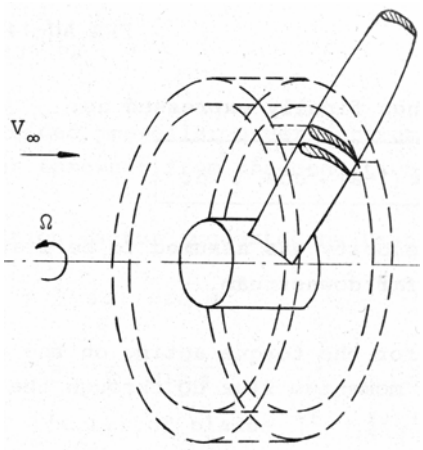

Figure 1 Annular ring generated by a blade element.

For steady flows, the relevant fundamental laws of fluid mechanics can be expressed as follows:

Force = mass flow * change in velocity from an upstream to a downstream position
Torque = mass flow * change in angular velocity downstream

1.1.1 Basic Axial Momentum Theory

Figure 2 shows the different velocities that are present when looking at the flow through a wind turbine.

V_∞ – free stream velocity
U – velocity at the turbine
V_2 – velocity after the turbine
V – reduced velocity due to turbine
a – axial induction factor = V/V_∞

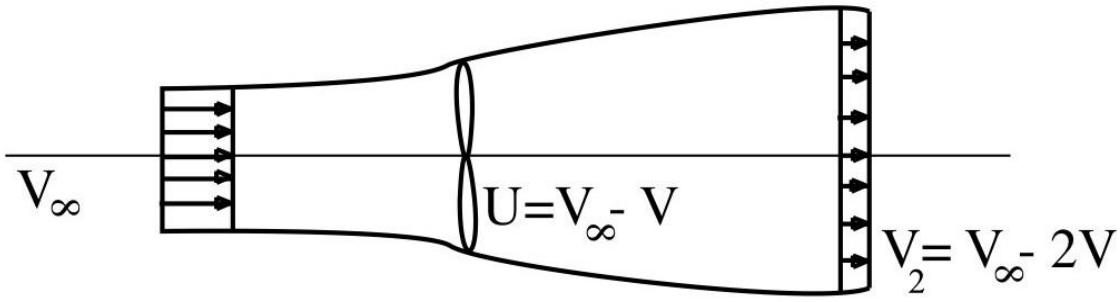

Figure 2 Flow through a wind turbine.

$U = V_\infty - V = V_\infty (1-a) \rightarrow V_2 = V_\infty (1-2a)$ (1)

Shaft power, P, of an ideal turbine can be obtained as the change per unit time in kinetic energy of the airflow through the turbine. P max is obtained when $dP/da = 0$

$$P_{max} = \frac{16}{27}\frac{1}{2}\rho A V_\infty^3 \quad (2)$$

$$Cp = \frac{P}{\frac{1}{2}\rho A V_\infty^3} \quad \text{(Definition of Cp)} \quad (3)$$

The maximum value of the power coefficient Cp would then be $16/27 \approx 0.59$

1.1.2 Blade Element Theory

Two velocity components act at radius *r* of a rotating blade element as can be seen in figure 3; the relative rotational speed experienced by the blade element,

r Ω (1+*a*') = r(Ω+ω) = r(turbine angular velocity + induced rotational angular velocity), where $a' = \frac{\omega}{\Omega}$ is the angular induction factor. The wind speed component is U in the axial direction. The resulting velocity vector is V_R.
There are also several angles to be considered which are also shown in figure 3:
Φ is the relative flow angle, θ is the blade angle that consists of the blade pitch angle θ_V and the local twist angle θ_T.
α is the angle of attack and equals Φ - θ.

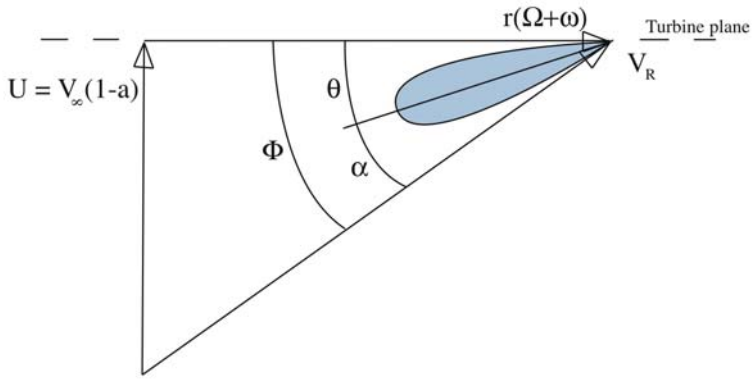

Figure 3 Velocities and angles acting on a blade element rotating at radius r.

The aerodynamic force components acting on the blade element (in 2D) are lift force dL perpendicular to the resulting velocity vector V_R and drag force dD acting in the direction of the resulting velocity vector. The corresponding aerodynamic coefficients then become

$$C_L = \frac{dL}{\frac{1}{2}\rho V_R^{\,2} c * dr} \qquad \text{(Lift coefficient)} \qquad (4)$$

$$C_D = \frac{dD}{\frac{1}{2}\rho V_R^{\,2} c * dr} \qquad \text{(Drag coefficient)} \qquad (5)$$

A projection of the forces in the turbine plane results in torque around the turbine axis. It will turn out to be of interest, with reference to the measurements treated below, to relate the so-called normal coefficient (C_N perpendicular to the chord line) and the chord line coefficient (C_T positive towards the leading edge) to the coefficients for lift and drag as follows

$$C_L = C_N \cos\alpha + C_T \sin\alpha \qquad (6)$$

$$C_D = C_N \sin\alpha - C_T \cos\alpha \qquad (7)$$

If the blade has a coning angle, Π, this is taken into account so that the radial distance includes the effect of Π.

The thrust force acting on the blade element is expressed as

$$dT = B * c * \frac{1}{2} * \rho * V_R^{\,2} * c_n * \cos\Pi * dr \qquad (8)$$

The torque around the turbine axis:

$$dQ = B * c * \frac{1}{2} * \rho * V_R^{\,2} * c_t * r * \cos^2\Pi * dr \qquad (9)$$

where
B = number of blades
c = chord length
r = radial coordinate of blade element
dr = radial extent of blade element
$c_n = C_N \cos\theta - C_T \sin\theta$
$c_t = C_N \sin\theta + C_T \cos\theta$

1.1.3 Momentum Theory for a Turbine with a Rotating Wake

This theory differs from the blade element method above, with regards to the calculation of thrust and torque. Expressions from both theories will be used in section 1.1.4. Here the axial thrust force dT can be expressed using the relations for momentum flux loss through the ring or Bernoulli's equation. Combining these expressions and using the relation in equation 1, the thrust force can be obtained as:

$$dT = 4\pi\rho * r * V_\infty^2 * a(1-a) * \cos^2\Pi * dr \qquad (10)$$

and the torque:

$$dQ = 4\pi\rho * r^3 * V_\infty * a'\Omega(1-a) * \cos^4\Pi * dr \qquad (11)$$

1.1.4 Tip and Hub Losses

Basic strip theory does not account for losses at the blade tip due to the airflow being unevenly distributed over the turbine disk. Prandtl's correction factor can then be used.

$$F_P = \frac{2}{\pi}\arccos e^{-f} \qquad (12)$$

Where for the tip region

$$f = \frac{B}{2}\frac{R-r}{R\sin\Phi} \qquad (13a)$$

and for the hub region

$$f = \frac{B}{2}\frac{r - r_{HUB}}{r_{HUB}\sin\Phi} \qquad (13b)$$

where
R = the total blade radius
r = the local blade element radius
r_{HUB} = the radius of the hub

The correction factor for total losses can actually be quite well represented by:

$$F_{tot} = F_p(tip) * F_p(hub) \qquad (14)$$

The equations derived by momentum theory for thrust and torque, equation 10 and 11, are then multiplied by F_{tot} before being equalized to the corresponding blade element expressions, equations 8 and 9 in section 1.1.2.

1.1.5 Calculation

Combining the blade element theory and the momentum theory, equations 8, 9, 10 and 11, results in:

$$dT(\text{blade element}) = dT(\text{momentum}) * F_{tot} \qquad (15)$$

$$dQ(\text{blade element}) = dQ(\text{momentum}) * F_{tot} \qquad (16)$$

Initial values for *a* and *a´* are assumed. Then values of *a* and *a´* are iterated until the BEM equations 15 and 16 are satisfied.

When this is finished for all blade elements, forces and moments are integrated over the entire blade and expressed both in a blade-fixed and in a turbine-fixed coordinate system.

Optimum wind turbine performance at a specified wind speed is obtained if each blade element has a chord and twist that maximize the local contribution to the power output.

This method is restricted to a wind turbine in a steady uniform free stream wind.

1.2 Potential Flow Dynamic Changes

Aerodynamic forces acting on a wing that moves suddenly from a steady situation to a constant vertical velocity, a so-called plunging, was studied by Wagner. The sudden change in angle of attack, that results from the plunging, does not lead to an instantaneous change in C_L according to the steady C_L/α curve.

Küssner examined the case where a wing travels into a sharp-edged gust striking the leading edge of an airfoil first. This gives a quick but gradual change of the angle of attack. Both these cases make the otherwise linear curve non-linear for a while until it stabilizes, if no further changes occur. See figure 4. This results in C_L that deviate from the steady curve.

Theodorsen then refined these concepts and made them more practical (see references 7 and 2).

1.3 Dynamic Stall

Dynamic stall is a dynamic delay of stall at higher angles of attack than the static stall angle. The phenomenon occurs on helicopter blades, rapidly manoeuvring aircraft, jet engine compressor blades and wind turbine blades as described in reference 4. In potential flow dynamic changes, the lift curve at low angles of attack was described as non-linear. This type of phenomenon also happens at the stationary stalling point, when the airfoil is exposed to a rapid change in the angle of attack. Instead of stalling at a certain angle of attack, the lift curve increases in a non-stable manner. As α stabilizes, C_L will return to the stationary curve. If the blade is oscillating between different angles, C_L will circulate around the stationary curve and the loop of the lift curve will not be symmetric. See figure 4.

Dynamic stall influences the loading of wind turbine rotors in several ways: it can give rise to vibrations and can have major consequences with respect to the structural behaviour.

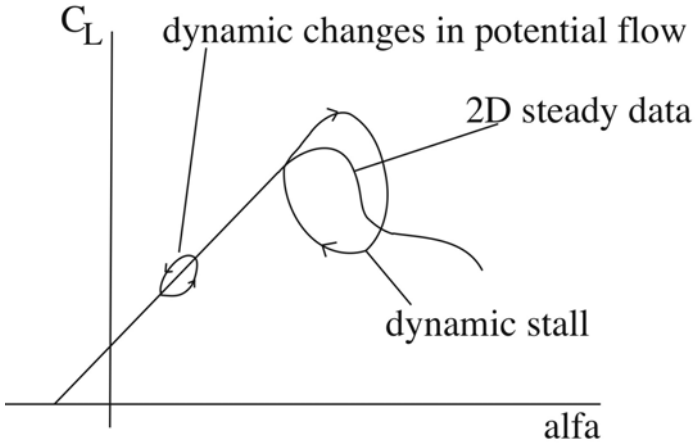

Figure 4 Dynamic changes.

At 30% (r/R = local radius/turbine radius) the dynamic stall effects are usually strong, there is not much agreement with 2D data and there is a large difference between the non-rotating and rotating cases. At 55%, 75% and 85% the agreement with 2D data is much closer but with some differences in the pressure distribution as shown in references 5 and 13.

Beddoes and Leishman (reference 10) have developed a method for dynamic stall, that is used in the present FFA method.

1.4 Weaknesses in Basic BEM

Tip losses – There is airflow around the blade tip due to pressure differences. This is historically referred to as a “loss” and it must be taken into account. For a lightly loaded propeller a method by Prandtl uses a correction factor (equations 12, 13a, 13b)

to compensate for the tip losses. Prandtl modelled the wake with a series of discs with the same screw thread pitch as that of the imaginary vortex sheet spiral. In reality there are no discs but Prandtl imagined a spiral with a surface of discontinuity from each blade on the turbine, like a double or triple threaded screw. That surface could be modelled as infinitely thin disks consisting of continuous ring vorticity. Prandtl's calculations only apply for optimum and stationary conditions. Goldstein, working directly with the vortex spiral surface model, made this spiral infinitely lightly loaded and applied complicated mathematics to it, but it does not apply to dynamic conditions. Theodorsen made a general development of Goldstein's theory and changed the infinite light load condition to allow an arbitrary load (an axial force, thrust).

Wind shear – The turbine is made for stationary flow. When the wind varies with height, the variation appears as a highly unsteady inflow condition to the individual blade element.

Turbulence – When small scale turbulence reaches the turbine, it creates different wind speeds at different points on the blades and this variation is not included in BEM. It is a type of dynamic inflow.

Dynamic inflow – When there is unsteady wind with large turbulence eddies or when quick pitching takes place, BEM underpredicts the true load variation that results.

Yaw – Yaw and yawing, as in the case of wind shear, causes sinusoidal loading, which is not correctly modelled using basic BEM.

Radial Distribution of Induced Wind – The rotor blade experiences an inflow that equals $V_\infty(1-a)$ where V_∞ is the wind speed and $a = \frac{v}{V_\infty}$ where v is the induced wind in the general flow direction. Figure 5 shows a as a function of r/R, (local radius/turbine radius). Counteracting model errors have concealed the approximation errors in Prandtl's theory.

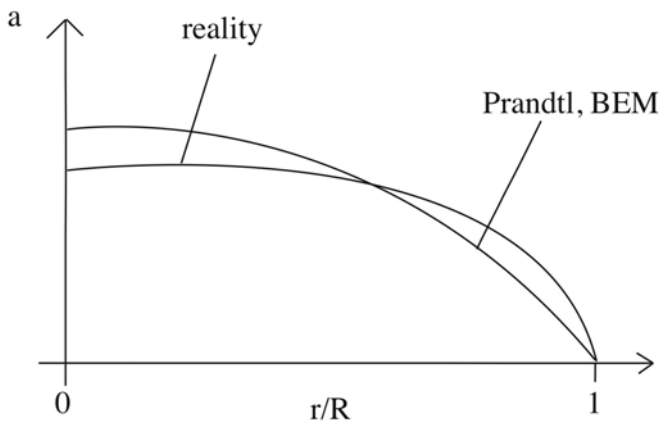

Figure 5 Radial induction distribution.

1.5 Vortex and Induction Theory

A vortex flow is a flow where all the streamlines are concentric circles about a given point. The velocity along any given circular streamline is constant, but it varies from one streamline to another inversely to the distance from the common center. The velocity components in the radial and tangential directions are $V_r = 0$ and V_θ = constant/ r, respectively.

The circulation from a given circular path of radius r is:

$$\Gamma = -\oint_C V \circ ds = -V_\theta (2\pi r) \qquad (17)$$

Γ is called the strength of the vortex flow.

According to the Kutta-Joukowski theorem (reference 1), the lift force per unit span can be calculated as $L = \rho V \Gamma$, where V is the wind velocity local to a bound vortex.

The fundamental equation for calculation of induced velocity is based on the Biot-Savart law (references 1 and 11):

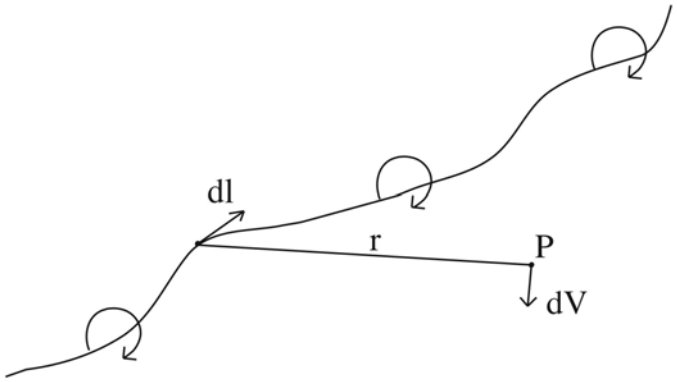

Figure 6 Vortex filament of strength Γ

The directed segment of the filament **dl** as shown in figure 6 induces a velocity at an arbitrary point P in space with a distance of the radius vector **d**. The velocity is calculated with the differential form of the Biot-Savart law (equation 18). In two dimensions the integral form becomes that of equation 19, also see figure 7.

$$dV = \frac{\Gamma dl \times d}{4\pi \left| d^3 \right|} \qquad (18)$$

$$w = \frac{\Gamma}{4\pi d} (\cos \varphi_A - \cos \varphi_B) \qquad (19)$$

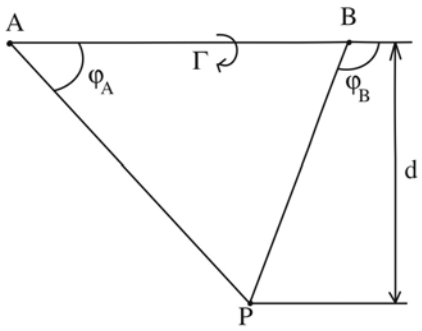

Figure 7 The included angles and distances in Biot-Savart's law from equation 19.

The law is a general result of potential theory and describes electromagnetic fields as well as inviscid, incompressible flows.

Helmholtz's theorems (reference 1) give that a vortex filament cannot end in a fluid; it must extend to the boundaries of the fluid or form a closed path, and that the strength of a vortex filament is constant along its length. If a finite wing of span b is replaced by a bound vortex and the vortex filament is assumed to continue as two free vortices trailing downstream from the wing tips to infinity, according to Helmholtz's theorem, a horseshoe vortex is formed. This horseshoe contributes to an induced downwash that increases when getting closer to the edges of the bound vortex. Instead of representing the wing by a single horseshoe vortex, a large number of horseshoe vortices can be used. Each with a different strength, but with all bound vortices on a lifting line. This results in a continuous vortex sheet trailing downstream of the lifting line. Any segment of the trailing vortex sheet will induce a velocity with a magnitude and direction given by the Biot-Savart law. The total velocity induced by the entire trailing vortex sheet is then the summation over all the vortex filaments.

The same idea also applies to turbines and propellers with the added complications caused by the rotation.

1.6 AERFORCE

AERFORCE is a subroutine package for the calculation of aerodynamic forces of wind turbine rotors (see reference 2). It is based on the BEM method and includes some extensions for dynamic inflow, inclined flow to the rotor disc and unsteady blade aerodynamics (dynamic stall effects). Its typical implementation is in aeroelastic computer code.

1.7 Himmelskamp

The stalling point, see figure 8, can be delayed when a propeller or turbine rotates. The boundary layer is exposed to centrifugal forces that will push the transition point back towards the trailing edge and result in less separated flow and more lift. The separated flow closest to the wing is dragged towards the tip of the blade due to centrifugal forces and due to backflow at the surface, a rotating field along the trailing edge is created. These effects get smaller further out towards the tip area, where there

is no or little separated flow. This rotating field of separated air is much more stable than separated flow on a non-rotating wing. This is called the Himmelskamp effect.

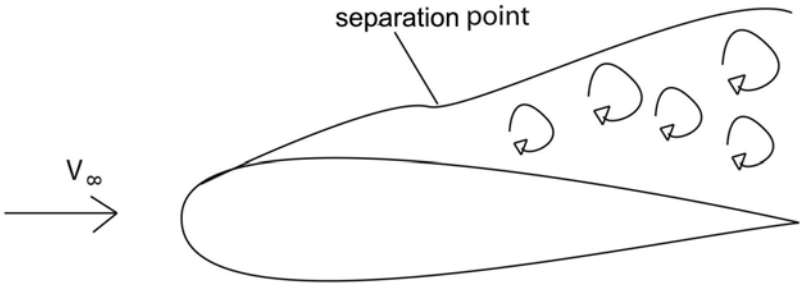

Figure 8 The separation point.

The lift force in the rotating case will be higher than for the 2D case. As can be seen in the (C_P)/chord graph in figure 9, the pressure is almost constant on top of the non-rotating blade, but for the rotating blade the pressure is gradually changing towards the trailing edge. This is the consequence of the centrifugal pumping, which could not take place unless there is a pressure gradient maintaining the pumped flow on the blade. This is an important fact to consider, when predicting aerodynamic forces on a wind turbine. Measurements have repeatedly given evidence of C_L-values in excess of 3.

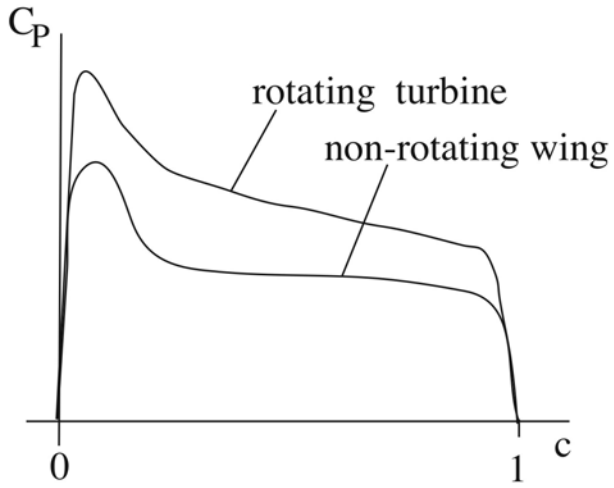

Figure 9 Himmelskamp's effect on the lift force.

H. Snel has given a formula (see reference 14) for the variation of C_L between 2D inviscid flow and 2D measured data. $C_{L,2D}$ and $C_{L,3D}$ in equation 20. $C_{L,inv}$ is the lift coefficient for inviscid flow.

$$C_{L,3D} = C_{L,2D} + f(C_{L,inv} - C_{L,2D}) \qquad (20)$$

f is a multiplication correction factor that depends on the ratio (c/r):

$$f = 3\left(\frac{c}{r}\right)^2 \qquad (21)$$

In 1981 Viterna and Corrigan developed an empirical model for modifying two-dimensional airfoil data to better represent wind turbine rotor behaviour (see reference 15). Their model said: In the attached flow regime there is no need for tip- or hub-loss models, in the high-lift/stall-development regime, the torque force does not decrease with increasing angle of attack and in the flat-plate/fully-stalled regime, the dominant parameter is the maximum value of the drag coefficient. Using the Viterna-Corrigan model gave a much better value of calculated power output. Although being a good approximation in the early 1980s, later application to modern slender blades showed less agreement with measurements, which indicates that the method is not general.

2. National Renewable Energy Laboratory (NREL)

The NREL is the U.S. Department of Energy laboratory for renewable energy research and development. Their national wind technology center has a database for unsteady aerodynamic experiments made available to participants in the IEA Annex XX international work group. The report that describes the test can be found in reference 9. A ten meter diameter wind turbine was tested in the largest wind tunnel in the world. The wind tunnel, which is located at NASA Ames Research Center, has a test section that is 24.4 m x 36.6 m and it is driven by six large fans each powered by a 22500-horsepower electric motor.

The wing section of the tested blade is constant with local radius station. The airfoil called S809, is developed by Airfoils, inc. and was designed to improve wind energy power production in stall-controlled wind turbines and to be less sensitive to leading edge roughness. It was equipped with 5 stations with pressure holes around the perimeter of the airfoil at 30%, 47%, 63%, 80%, and 95%. There were also five probes along the blade, protruding from the leading edge and located at 34%, 51%, 67%, 84%, and 91% radius, see figure 10.

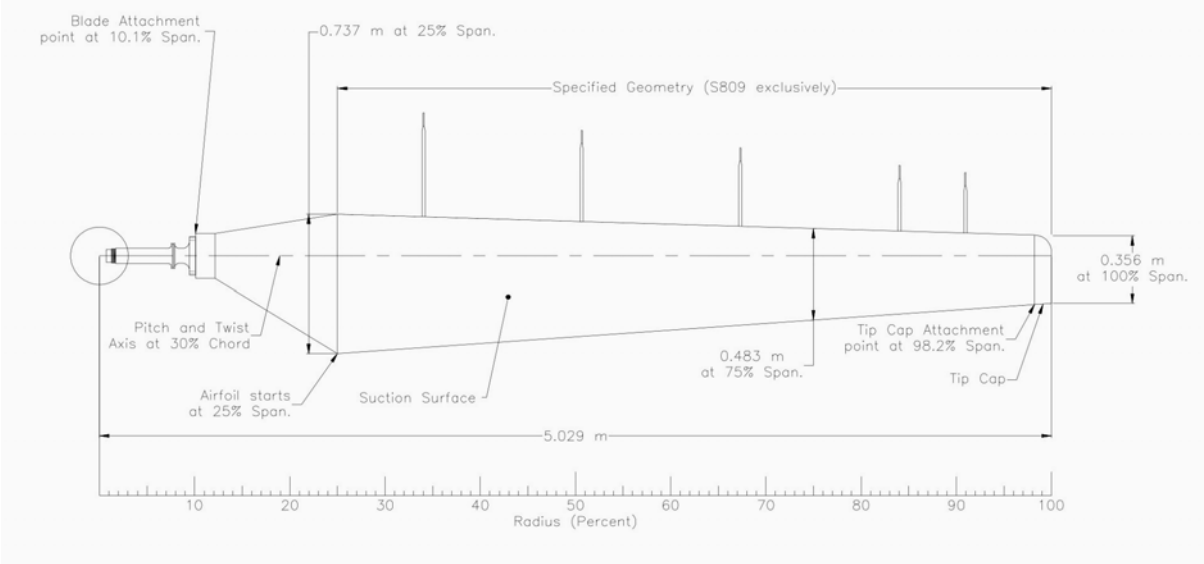

Figure 10 Blade plan form dimensions.

At each pressure tap station C_N, C_T, C_M, and C_{Th} was obtained and at each probe station the dynamic pressure and the local flow angle could be measured. Also wind tunnel data like air density, velocity, rotational speed and tip angle can be found in the database. The probe is illustrated in figure 11.

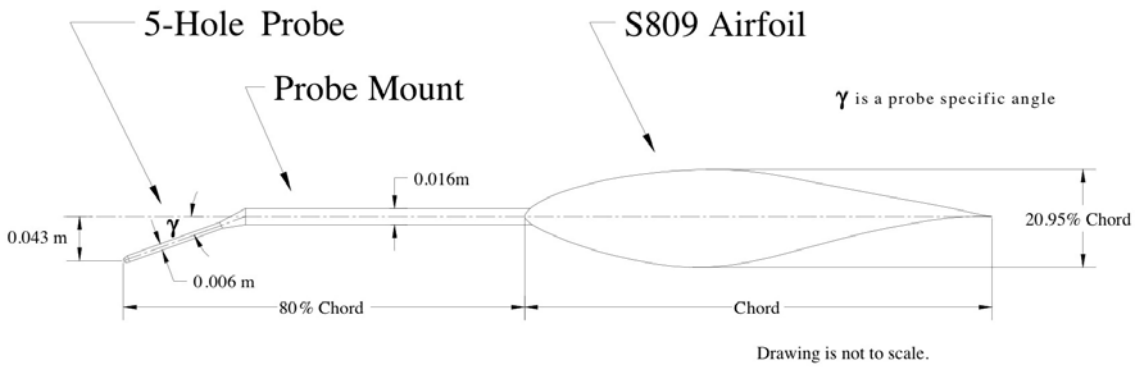

Figure 11 Blade-mounted five-hole probe

In order to calculate C_L, which is necessary to obtain any results of this thesis, the angle of attack must first be determined. The data that was used from the database at NREL was from an upwind baseline sequence, where the turbine was rigid with a 0° cone angle. The wind speed ranged from 5 m/s to 25 m/s, the yaw angle was at 0° and the blade tip pitch at 3°, which is considered to be the standard operating condition. The rotor rotated at 72 RPM.

3. Calculating the Angle of Attack by the BEM Method

Here the basic BEM method, described in section 1.1, is applied to the S809 blade with the purpose of finding the induction *a*. The results are presented in appendix A. Since the information on the aerodynamic coefficients is collected from the pressure stations, the friction drag is not included and must be added, see equation 22. The friction drag was obtained from Xfoil and then extrapolated for large angles of attack. Xfoil is an interactive program for subsonic airfoil development that can be downloaded free from the internet at http://raphael.mit.edu/xfoil/. The S809 airfoil coordinates were given by the NREL reference 9.

In order to calculate *a*, the following equations are needed and are combined in equation 28.

$$C_{Th} = C_N \cos\theta - C_T \sin\theta + C_{Df} \sin(\alpha + \theta) \tag{22}$$

where C_{Df} is the friction drag coefficient and C_{Th} the thrust coefficient.

$$\Delta Th = C_{Th} * \frac{1}{2} \rho V_R^2 * c * \Delta r * B \qquad \text{(Blade element theory)} \tag{23}$$

$$\Delta Th = \Delta \dot{m} * F_{tot} * 2a * V_\infty = \rho \pi (r_y^2 - r_i^2) * 2F_{tot} a V_\infty^2 (1-a)$$
$$\text{(Momentum theory)} \tag{24}$$

where

$$(r_y^2 - r_i^2) = \Delta r * 2r \tag{25}$$

From figure 3 the following expression is readily obtained.

$$V_R^2 = \left(\omega r(1+a')\right)^2 + \left(V_\infty(1-a)\right)^2 \tag{26}$$

To calculate F_{tot}, as described in section 1.1.4, the angle Φ is needed.

$$\Phi = \arctan\left(\frac{V_\infty(1-1.5a)}{\omega r(1+a')}\right) \tag{27}$$

Equation 23 and 24 are set equal and combined with equation 25, 26 and 27. The result is equation 28.

$$a = \frac{C_{Th} * V_R^2 * c * B}{8\pi r * V_\infty^2 * F_{tot}(1-a)} \tag{28}$$

Equation 28 is then used in Excel with the function Solve to obtain *a*. *a'* is set to depend on *a* as equation 29.

$$a' = \frac{1}{2}\left((-1) + \sqrt{1 + \frac{4a(1-a)}{(\lambda x)^2}}\right) \tag{29}$$

α is then found geometrically as:

$$\alpha = \arccos\left(\frac{\omega r(1+a')}{V_R}\right) - \theta \tag{30}$$

4. Calculation of the Angle of Attack Using Probe Information

To calculate the angle of attack from probe data, the lifting line theory was used. Small pieces of lifting lines with a certain circulation, Γ, induce velocities at the probe heads. These velocities were then added. For further description see section 1.5 and referece 1. From the database information, the local velocity and the local flow angle (LFA) at the probe head were obtained. By calculating them as precisely as possible and minimizing the error, the angle of attack, α, was obtained. See appendix B for the results.

An α first had to be guessed, so a start value of C_L gave the circulation Γ as:

$$C_L = C_N*\cos(\alpha) + C_T*\sin(\alpha) \quad (31)$$

$$\Gamma = \frac{1}{2} * V_{R2} * c * C_L \quad (32)$$

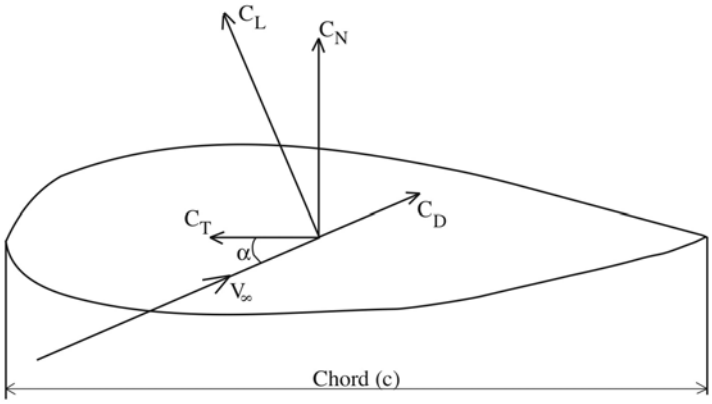

Figure 12 Relationship between C_N, C_T, C_D and C_L.

The relationship between C_N, C_T and C_L can be seen in figure 12. In equation 32 the velocity is defined as:

$$V_{R2} = \sqrt{\left(V_\infty(1-a_2)\right)^2 + (\omega r_2(1+a'_2))^2} \quad (33)$$

a and *a'* are collected from equations 40 and 42, the rotational speed, ω, from the data base and r_2 is the local radius to the end point of the distance *s*, seen in figure 13, where the lifting line will be located. Since C_N and C_T are taken from pressure taps, the circulation points will be located at the same stations: 30%, 47%, 63%, 70%, and 95% of the radius, and at the distance *s* from the leading edge. Equations 34 and 35 describe the distance *s*.

$$C_m = -C_N * \frac{x}{c} \quad (34)$$

$$s = x + 0.25c = c\left(-\frac{C_m}{C_N} + 0.25\right) \quad (35)$$

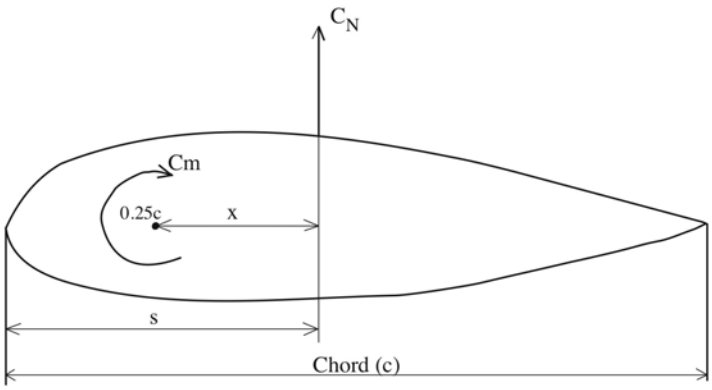

Figure 13 Distance *s* from the leading edge.

The definition of *a* and *a'* are given by figure 14 according to reference 18. Theodorsen claims that an induced velocity in the very far wake will be perpendicular to the helical vortex sheet. Applying this idea directly on the blade, explains the square angle in figure 14. The angle θ in figure 14 is the twist angle plus the pitch angle. The twist angle is obtained from table 1. Since the tip twist angle is –1.8°, 4.8° must be added to obtain the blade tip pitch that is 3.0°. The angle θ is then equal to twist angle plus 4.8°.

Table 1 Chord and twist along the blade.

Span Station (r/5.029 m)	**Chord Length (m)**	**Twist (degrees)**
0.0	Hub - center of rotation	Hub - center of rotation
0.101	0.218 (root hub adapter)	0.0 (root hub adapter)
0.131	0.218	0.0
0.176	0.183	0.0
0.200	0.349	6.7
0.212	0.441	9.9
0.225	0.544	13.4
0.250	0.737	20.040
0.267	0.728	18.074
0.300	0.711	14.292
0.328	0.697	11.909
0.388	0.666	7.979
0.449	0.636	5.308
0.466	0.627	4.715
0.509	0.605	3.425
0.570	0.574	2.083
0.631	0.543	1.150
0.633	0.542	1.115
0.691	0.512	0.494
0.752	0.482	-0.015
0.800	0.457	-0.381
0.812	0.451	-0.475
0.873	0.420	-0.920
0.934	0.389	-1.352
0.950	0.381	-1.469
0.994	0.358	-1.775
1.0	0.355	-1.816

Equation 36 is geometrically taken from figure 14 and then *a* and *a'* can be calculated using equations 36 to 42.

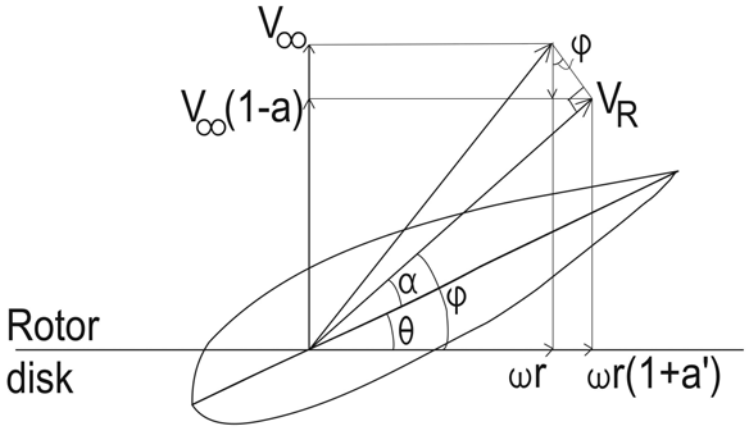

Figure 14 Velocities including *a* and *a'* according to Theodorsen (1948).

$$\frac{\omega r a'}{V_\infty a} = \tan\varphi = \frac{V_\infty (1-a)}{\omega r (1+a')} \tag{36}$$

$$\text{def: } \frac{\omega r}{V_\infty} = \frac{\omega R}{V_\infty} * \frac{r}{R} = \lambda x \tag{37}$$

$$\because\ a'(1+a') = \frac{a(1-a)}{(\lambda x)^2} \tag{38}$$

$$a'^2 + a' - \frac{a(1-a)}{(\lambda x)^2} = 0 \tag{39}$$

$$\because\ a' = \frac{1}{2} * \left(-1 + \sqrt{1 + \frac{4a(1-a)}{(\lambda x)^2}} \right) \tag{40}$$

Equation 36 combined with equations 37 and 40 gives for *a*

$$1 + \frac{4a(1-a)}{(\lambda x)^2} = \left(\frac{1-a}{\frac{1}{2}\lambda x \tan\varphi} - 1 \right)^2 \tag{41}$$

which leads to

$$\because\ a = \frac{1 - 2\tan\varphi * \frac{1}{2}\lambda x}{\tan^2\varphi + 1} = \cos\varphi(\cos\varphi - \lambda x \sin\varphi) \qquad (42)$$

a and *a'* are then used in equation 33. The different local radii to the locations of the lifting line, will give unique *a* and *a*' values for the different points.

An interpolated curve of Γ along the blade radius is then used as the lifting line, see figure 15. It is divided into 8 sections with limits at 13%, 23%, 30%, 47%, 63%, 80%, 95%, 98%, and 100% radius. An average, valid over the span of a section, is then calculated at each section and is used to obtain the induced velocities, *w*, at each probe, due to the circulation on the blade.

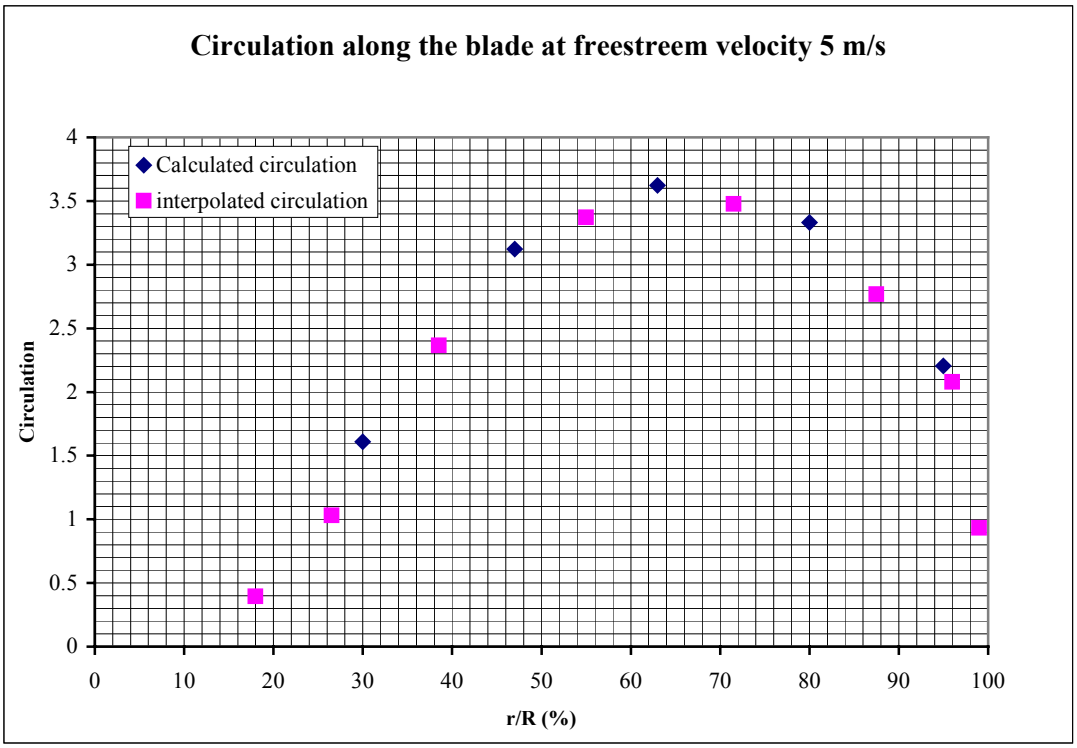

Figure 15 An interpolated curve of Γ along the blade radius.

Biot-Savart's law for two dimensions is given by equation 43 and then the sum of all induced velocities at each probe are added together. Also interactions from the lifting lines of the other blade are added (w_{B2}).

$$w = \frac{\Gamma}{4\pi d}(\cos\varphi_A - \cos\varphi_B) \qquad (43)$$

If the angle that occurs in three dimensions *d* is ignored, there will only be an error of 0.3% because of very small angular variations. See figure 16.

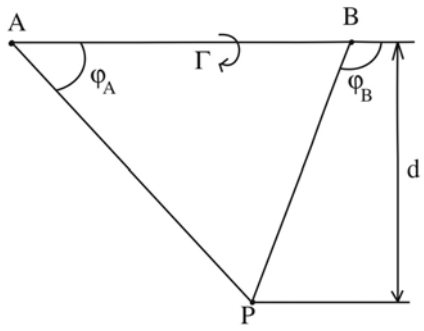

Figure 16 Scheme for Biot-Savart's law.

Since the probe is only 80% of the chord ahead of the body of the blade, the body will also induce a velocity on the end of the probe. This velocity was obtained by the program solidBody (see Appendix D). The velocity was given in the x and y directions in the chord plane as equations 44 and 45 show. They describe how α (in degrees) varies with w_x and w_y. These were then added to all sums of w obtained through the lifting line theory and w_{B2} from the other blade to obtain w_{tot} in equation 47. Also see figure 17.

$$w_x = -0.0015\alpha - 0.176 \tag{44}$$

$$w_y = -9*10^{-5}\alpha^2 + 0.0197\alpha - 0.0797 \tag{45}$$

The angle κ that is shown in fig. 17 is a geometric angle where 0.043 is the perpendicular distance between the chord line and the probe head and s is shown in fig. 13. The angle is given by equation 46.

$$\kappa = \arctan\left(\frac{0.043}{0.8*c+s}\right) + \theta \tag{46}$$

$$w_{tot} = \sqrt{\left((w+w_{B2})\cos\kappa + w_y\cos\theta - w_x\sin\theta\right)^2 + \left((w+w_{B2})\sin\kappa + w_x\cos\theta + w_y\sin\theta\right)^2} \tag{47}$$

$$\Psi = arc\cot\frac{(w+w_{B2})\cos\kappa + w_y\cos\theta - w_x\sin\theta}{(w+w_{B2})\sin\kappa + w_x\cos\theta + w_y\sin\theta} \tag{48}$$

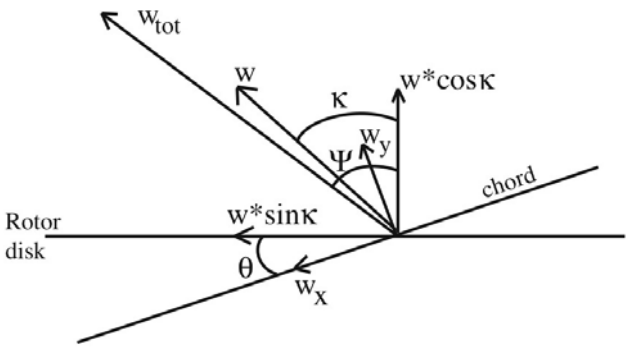

Figure 17 The relation between the induced velocities and w_{tot}

LFA (ξ in figure 18) can be obtained geometrically through the values of w_{tot} as:

$$V_{D,ber} = \sqrt{\left(\omega r_1(1+a_1') - w_{tot}\sin\Psi\right)^2 + \left(V_\infty(1-a_1) + w_{tot}\cos\Psi\right)^2} \quad (49)$$

$$\beta = \arccos\left(\frac{\omega r_1(1+a'_1) - w_{tot}\sin\Psi}{V_{D,ber}}\right) \quad (50)$$

$$LFA_{Ber} = \beta - \theta \quad (51)$$

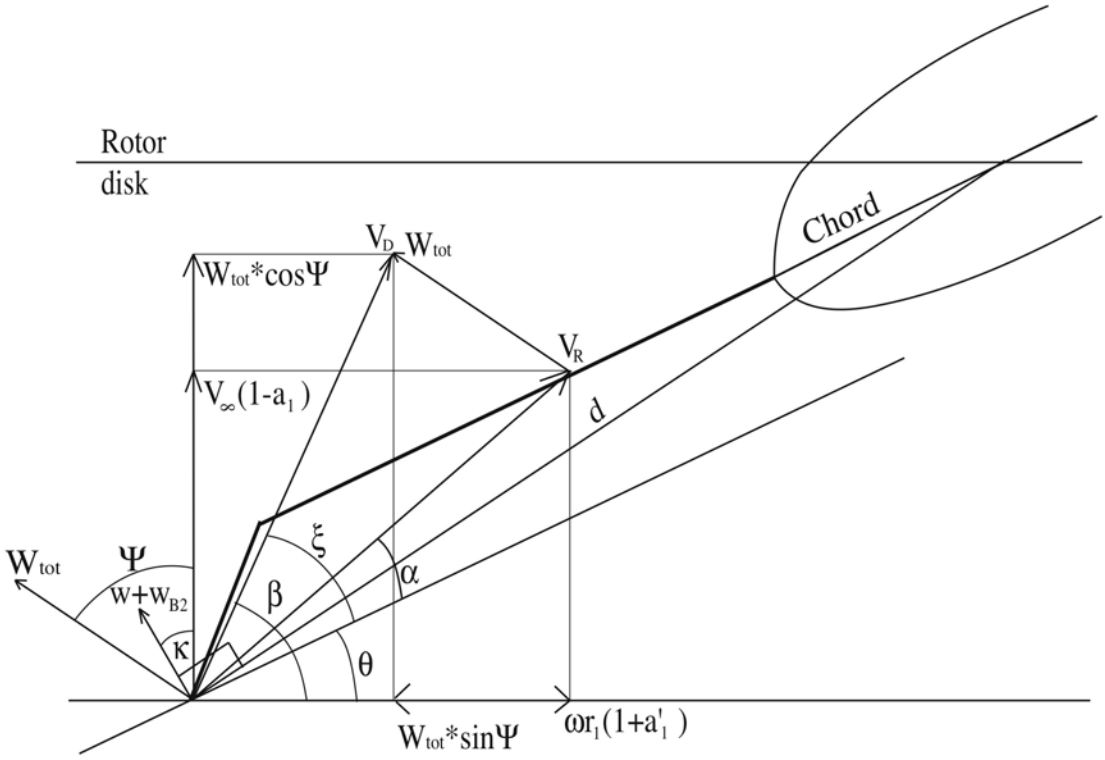

Figure 18 Probe velocities and angles.

The calculated LFA is subtracted from the LFA obtained from the data base information. The difference should be as small as possible, and by using the Excel function Solve to obtain this minimum and choosing α as the parameter to be varied, the minimum is obtained.

The calculated V_D is also compared with the velocity obtained from the dynamic pressure. It should be a bit smaller since the velocity from the database also has a sideways local flow angle.

5. Calculation of the Angle of Attack from 2D-data

Since C_N and C_T are known from the NREL database, a chart can be drawn comparing the angle of attack that is to be found with two-dimensional data taken from Appendix C. For low velocities and low angles of attack the two curves cross each other. The angle of attack is at the intersection between the curve, derived from the NREL tests (almost horizontal – see Eq. (31)), and the 2D curves, see figure 19. To check the 2D-curves from the different universities, in appendix C, the program XFOIL was used for comparison.

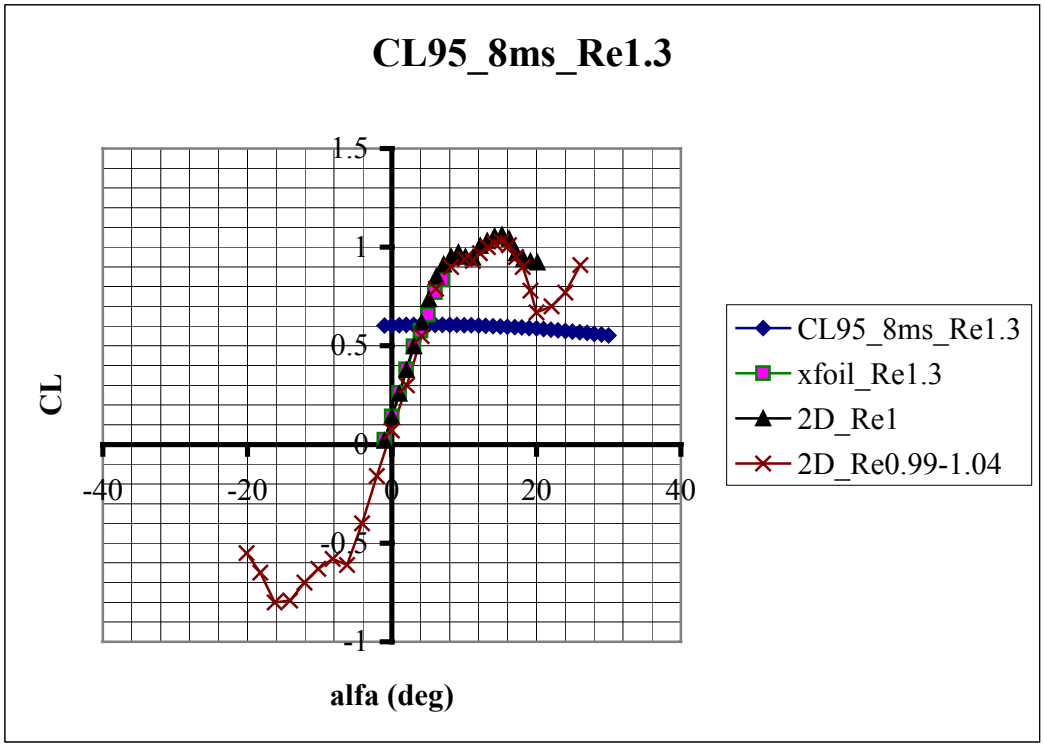

Figure 19 - Intersection with the 2D-curves.

When examining a station close to the hub at the blade, there is no intersection with the two-dimensional curves, see figure 20. Instead, a line extending from the linear part of the 2D curves was used to extrapolate the 2D-curve so an intersection could be estimated. This method is recognized to be extremely inaccurate. But, for lack of a better method it was explored.

It can be stated that the larger the distance between the 2D curves and the curve from the NREL measurements (diamonds) the larger the Himmelskamp effect.

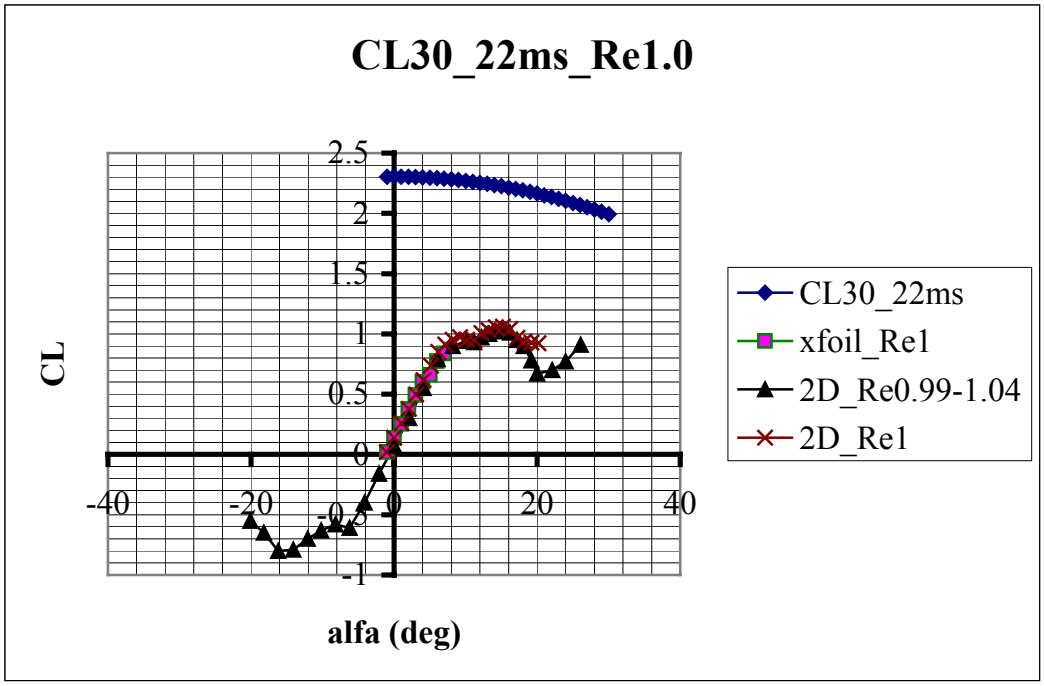

Figure 20 The Himmelskamp effect is so strong that an intersection can not be seen.

6. Results and Conclusions

The target of finding any connections between 2D-, 3D-data and the angle of attack was not achieved. This is shown to be a tough assignment when not even NREL in "*Peak and Post-Peak Power Aerodynamics from Phase VI NASA Ames Wind Turbine Data*" by Brandon S. Gerber, April 2004, could find a conclusion.

An attempt to find the angle of attack was made by trying to create a relation between the local flow angle (LFA) and the angle of attack. This was shown to be possible at low wind tunnel speeds but at high speeds the 2D and 3D effects was shown to be too different as can be seen in figure 21.

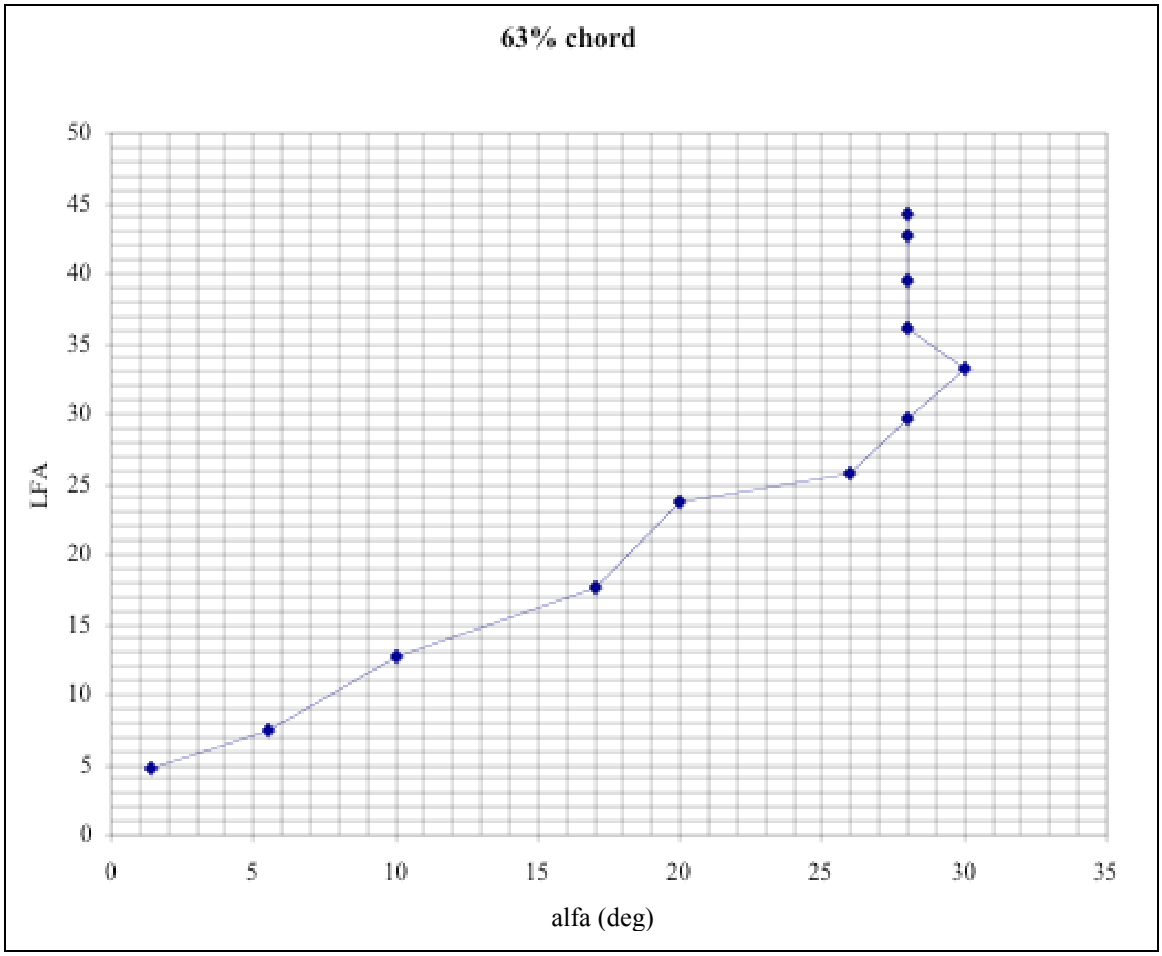

Figure 21. Relation between LFA and the angle of attack.

For all the three methods, described in sections 3 to 5, charts were made for comparison. Each chart is for a specific station at the blade, 30%, 47%, 63%, 80%, or 90%. It can clearly be seen that the factor (c/r), from equations 20 and 21, has a large impact on the curves close to the hub and they are not two-dimensional. Closer to the tip of the blade, the curves merge and appear more likely to be two-dimensional. See figures 22 to 26.

Each point in the charts represents an individual free stream velocity. This means that the Reynolds number varies along the C_L curve from about 0.8 millions to 1.3 millions.

The curves are named:
alfa BEM: the calculations in section 3.
alfa probe: the calculations in section 4.
alfa crossing lfa: the calculations in section 5.
xfoil_Re 1 milj.: the calculations made with the program XFOIL.
2D_Re 1 milj.: the data acquired from the tables in Appendix C.

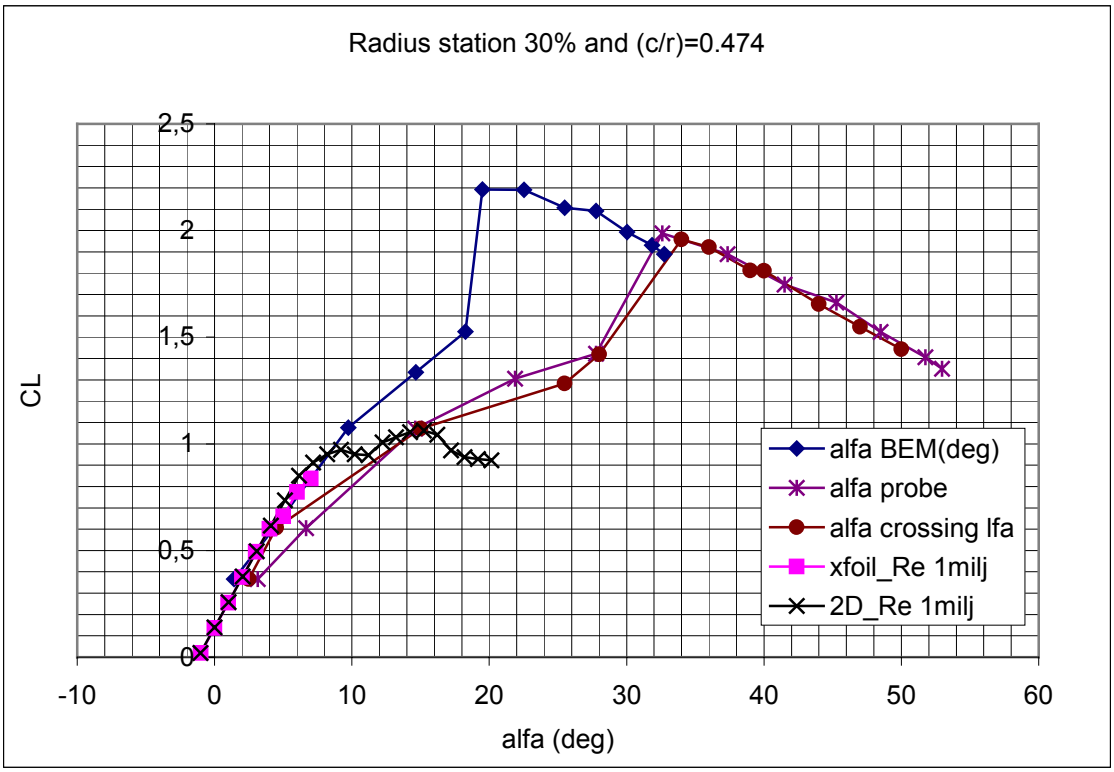

Figure 22

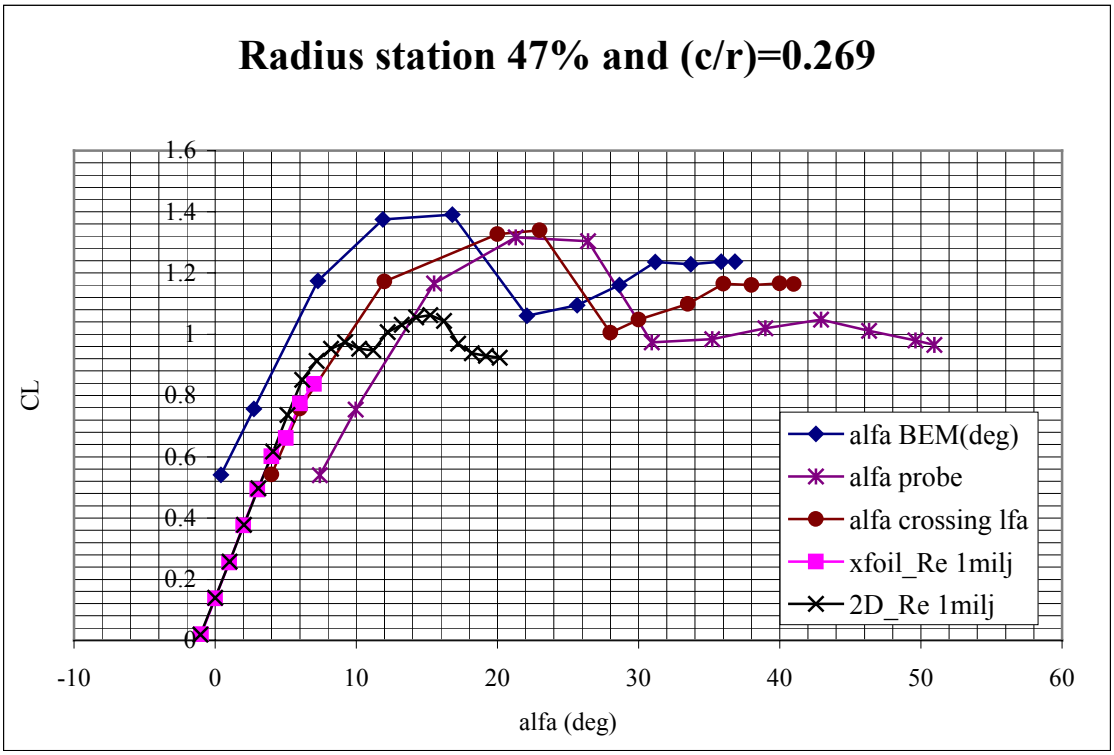

Figure 23

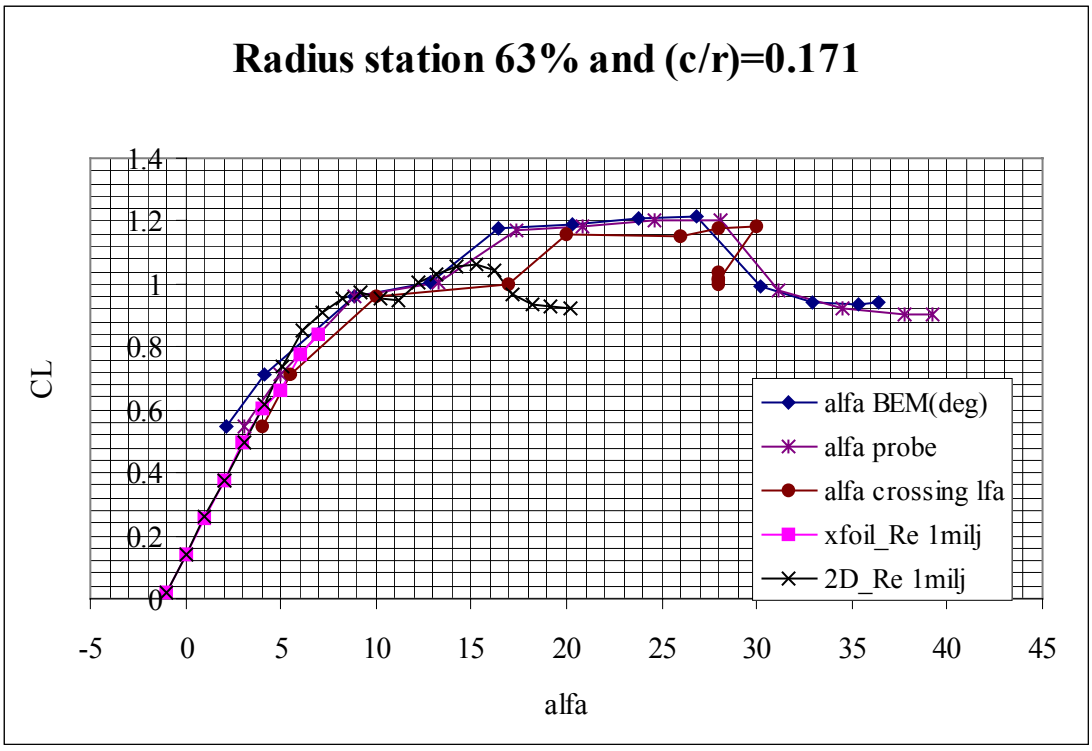

Figure 24

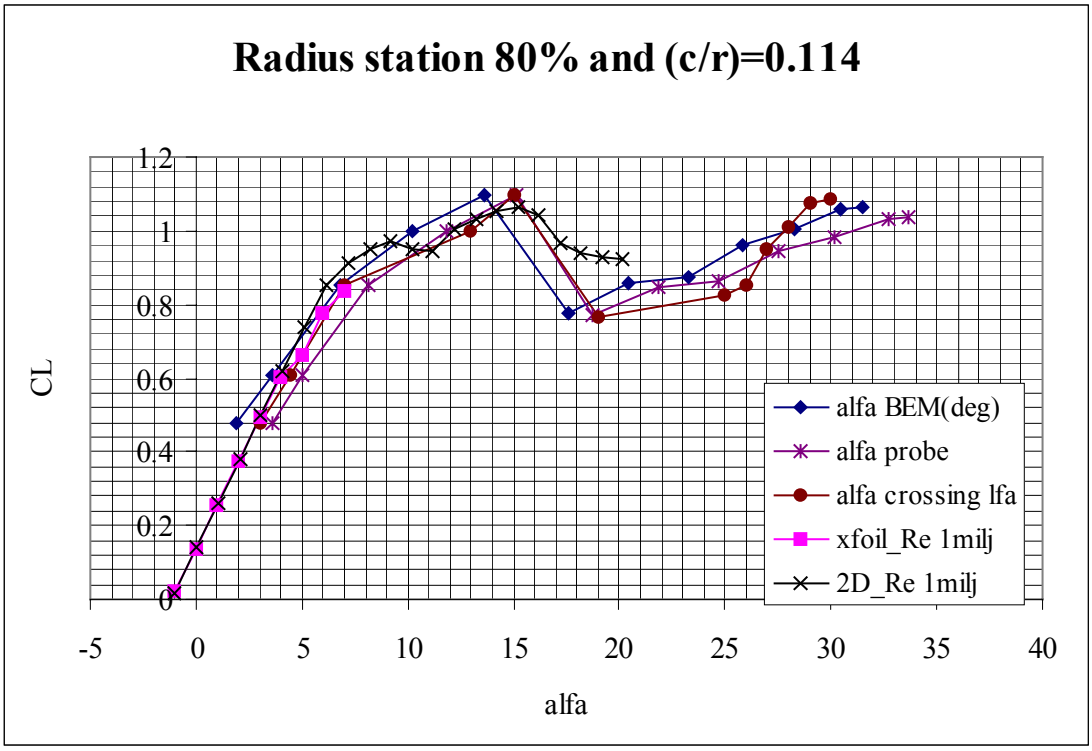

Figure 25

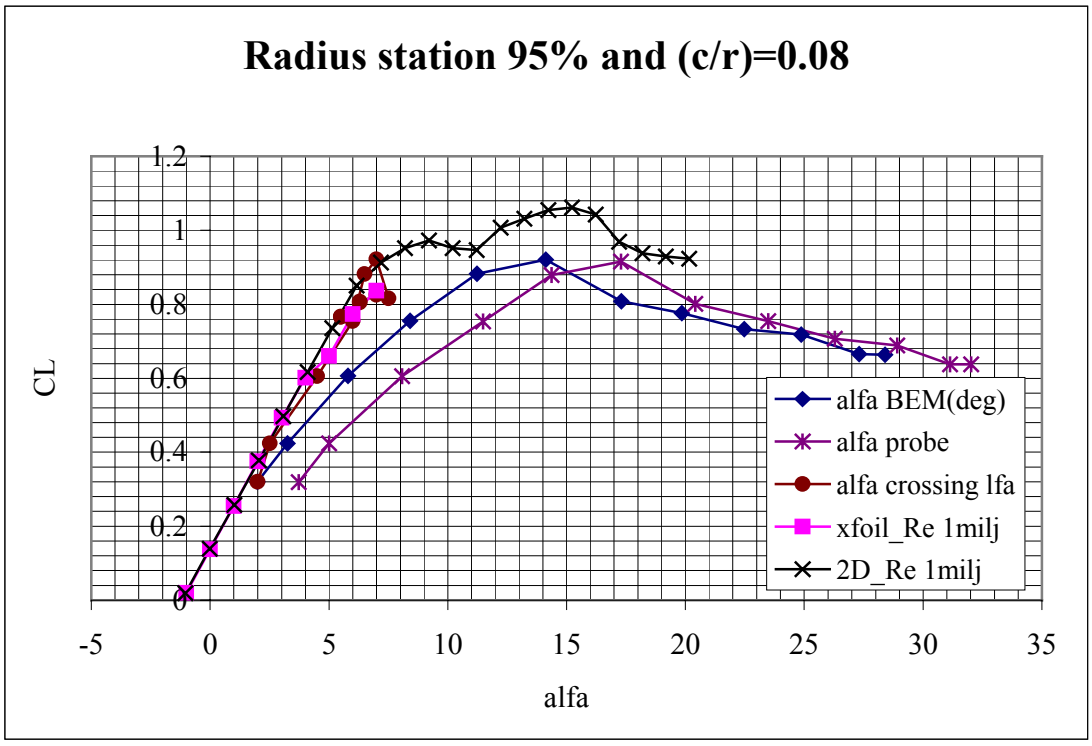

Figure 26

References

[1] Anderson, J.D Jr., *Fundamentals of Aerodynamics*, McGraw-Hill, Third Edition, Singapore, 2001

[2] Bisplinghoff, R. L., Ashley, H., Halfman, R. L., *Aeroelasticity*, Addison-Wesley publishing company, Cambridge, 1955.

[3] Björck, A., *AERFORCE: Subroutine Package for Unsteady Blade-Element/Momentum Calculations*, FFA, FFA TN 2000-07, Bromma, 2000.

[4] Björck, A., *Dynamic Stall and Three-dimensional Effects*, FFA TN 1995-31, Bromma, 1995.

[5] Björck, A., Ronsten, G., Montgomerie, B., *Aerodynamic Section Characteristics of a Rotating and Non-rotating 2.375 m Wind Turbine Blade*, FFA, FFA TN 1995-03, Bromma, 1995.

[6] Freris, L.L, *Wind Energy Conversion Systems,* Prentice Hall International (UK) Ltd, Cambridge, 1990

[7] Fung, Y.C., *An Introduction to the Theory of Aeroelasticity,* Dover publications, New York, 1993.

[8] Gustafsson, A., Lundgren, S., Frisk, B., *Application of a Method for Aerodynamic Analysis and Design of Horizontal Axis Wind Turbines*, FFA, Technical note AU-1499, Stockholm, 1980.

[9] Hand, M.M., Simms, D.A., Fingersh, L.J., Jager, D.W., Cotrell, J.R., Schreck, S., Larwood, S.M., *Unsteady Aerodynamics Experiment Phase VI: Wind Tunnel Test Configurations and Available Data Campaigns,* National Renewable Energy Laboratory, NREL/TP-500-29955, Golden Colorado, December 2001

[10] Leishman, J. G., Beddoes, T. S., *A Semi-empirical Model for Dynamic Stall*, Journal of the American Helicopter Society, July 1989.

[11] Montgomerie, B., *Dynamic Stall Model Called "Simple"*, Netherlands Energy Research Foundation ECN, ECN-C--95-060, Petten, 1996.

[12] Ronsten, G, *Geometry and Installation in Wind Tunnels of a STORK 5.0 WPX Wind Turbine Blade Equipped with Pressure Taps,* FFA, FFAP-A 1006, Bromma, 1994

[13] Ronsten, G, *Static Pressure Measurements on a Rotating and a Non-rotating 2.375 m Wind Turbine Blade Comparison with 2D Calculations,* FFA, FFA TN 1991-36, Stockholm, 1991

[14] Snel, H., Houwink, R., Bosschers, J., *Sectional Prediction of Lift Coefficients on Rotating Wind Turbine Blades in Stall*, Netherlands Energy Research Foundation ECN, ECN-C--93-052, Petten, 1994.

[15] Spera, D. A., *Wind Turbine Technology, Fundamental Concepts of Wind Turbine Engineering*, American Society of Mechanical Engineers, New York, 1994.

[16] Snel, H., Schepers, J.G (ed.), *JOULE1: Joint Investigation of Dynamic Inflow Effects and Implementation of an Engineering Method*, ECN-C-94-107, 1994

[17] Schepers, J.G., Snel, H. (ed.), *JOULE2: Dynamic Inflow: Yawed Conditions and Partial Span Pitch*, ECN-C-95-056, 1995

[18] Theodorsen, T., *Theory of Propellers,* Publications in Aeronautical Science, McGraw-Hill Publications, New York 1948.

Appendix A - Results from the BEM Method.

Table 2. Free wind velocity 5 m/s

r/R (%)	V_R	*a*	*a*'	alfa (deg)	Ftot
30	12.4146474	0.0976	0.01674	4.010476	0.9151
47	18.4812071	0.1996	0.01242	4.905368	0.9605
63	24.3747107	0.2435	0.00801	4.776967	0.9625
80	30.7206039	0.2356	0.00487	4.547179	0.904
95	36.3488218	0.2301	0.0034	4.579131	0.6104

Table 3. Free wind velocity 6 m/s

r/R (%)	V_R	*a*	*a*'	alfa (deg)	Ftot
30	12.835829	0.12154	0.02887	6.944414	0.8946
47	18.7637	0.19889	0.01775	7.242806	0.9388
63	24.592874	0.22174	0.01077	6.795429	0.9335
80	30.895296	0.21125	0.00648	6.211143	0.8572
95	36.493322	0.22258	0.00478	5.843507	0.5627

Table 4. Free wind velocity 8 m/s

r/R (%)	V_R	*a*	*a*'	alfa (deg)	F
30	13.84314795	0.1444	0.05776	12.3353	0.857
47	19.46587221	0.1931	0.03047	11.7678	0.894
63	25.161901	0.1486	0.01399	11.5561	0.855
80	31.33547894	0.1835	0.01031	9.43216	0.778
95	36.86071449	0.2084	0.00807	8.39299	0.492

Table 5. Free wind velocity 10 m/s

r/R (%)	V_R	*a*	*a*'	alfa (deg)	F
30	15.040467	0.1469	0.08895	15.45431	0.8138
47	20.347014	0.1734	0.04325	14.57076	0.8352
63	25.859963	0.1301	0.01945	13.70741	0.792
80	31.90129	0.1516	0.01379	11.02369	0.6979
95	37.332774	0.1913	0.01178	9.210551	0.4269

Table 6. Free wind velocity 12 m/s

r/R (%)	V_R	*a*	*a*'	alfa (deg)	F
30	16.359204	0.1574	0.13056	20.8743	0.8001
47	21.401234	0.1382	0.05136	21.2965	0.7992
63	26.684884	0.1226	0.02644	19.0891	0.7595
80	32.583543	0.1241	0.01674	16.2179	0.6552
95	37.912775	0.1647	0.01504	13.8314	0.3969

Table 7. Free wind velocity 14 m/s

r/R (%)	V_R	*a*	*a'*	alfa (deg)	F
30	17.67651	0.1985	0.20073	22.10285	0.7984
47	22.60865	0.0925	0.04935	26.59213	0.7545
63	27.64349	0.1002	0.03006	22.96032	0.7189
80	33.38985	0.0745	0.01449	20.23211	0.6011
95	38.59334	0.1379	0.01764	16.72444	0.3632

Table 8. Free wind velocity 16 m/s

r/R (%)	V_R	*a*	*a'*	alfa (deg)	F
30	19.191424	0.1907	0.24519	25.1334	0.7787
47	23.886206	0.0863	0.05997	30.136	0.7313
63	28.704435	0.0885	0.03496	26.3867	0.6888
80	34.271095	0.0725	0.01837	23.059	0.5738
95	39.376444	0.102	0.01775	19.9012	0.3337

Table 9. Free wind velocity 18 m/s

r/R (%)	V_R	*a*	*a'*	alfa (deg)	F
30	20.803173	0.1772	0.28424	28.0935	0.7599
47	25.24987	0.0847	0.07364	33.1318	0.714
63	29.857948	0.0821	0.0411	29.4473	0.6657
80	35.247018	0.0657	0.02117	25.8972	0.5497
95	40.227393	0.0927	0.02057	22.4528	0.3161

Table 10. Free wind velocity 20 m/s

r/R (%)	V_R	*a*	*a'*	alfa (deg)	F
30	22.44668	0.1701	0.32853	30.3809	0.7467
47	26.68545	0.0853	0.09011	35.6802	0.7007
63	31.11311	0.0647	0.04074	32.8092	0.6422
80	36.30265	0.0647	0.02566	28.415	0.5314
95	41.16386	0.0789	0.02192	25.0856	0.3004

Table 11. Free wind velocity 22 m/s

r/R (%)	V_R	*a*	*a'*	alfa (deg)	F
30	24.15801	0.1597	0.36716	32.6274	0.7341
47	28.19662	0.0811	0.10297	38.2037	0.6882
63	32.43285	0.0581	0.04441	35.5634	0.626
80	37.43616	0.0623	0.02984	30.8392	0.5156
95	42.17044	0.0715	0.02417	27.4738	0.2885

Table 12. Free wind velocity 24 m/s

r/R (%)	V_R	*a*	*a*'	alfa (deg)	F
30	25.88973	0.1529	0.40911	34.44733	0.7246
47	29.75762	0.0794	0.11847	40.34602	0.6785
63	33.81545	0.0549	0.04992	37.97408	0.6133
80	38.63717	0.0618	0.03508	33.04493	0.5028
95	43.25076	0.0611	0.02483	29.90075	0.2777

Table 13. Free wind velocity 25 m/s

r/R (%)	V_R	*a*	*a*'	alfa (deg)	F
30	26.77311	0.1489	0.42842	35.33399	0.7201
47	30.55615	0.0785	0.12637	41.33339	0.6743
63	34.52812	0.0542	0.05328	39.07152	0.6079
80	39.26306	0.0606	0.03729	34.13600	0.4968
95	43.81307	0.0583	0.0258	31.00118	0.2734

Appendix B - Results from the Calculations with the Probe Information Included.

Table 14. Free wind velocity 5 m/s

r/R(%)	alfa(deg)	C_L:	Circulation	a'_2	a_2
30	3.138239317	0.365443038	1.611495318	0.010743397	0.05978016
47	7.418893986	0.53997445	3.122741198	-0.00601561	-0.070933352
63	3.079326672	0.546001607	3.627010054	0.007810846	0.234840547
80	3.576284098	0.477019241	3.335399535	0.003395702	0.147027838
95	3.721173689	0.319375621	2.206555275	0.001898002	0.111026039

r/R(%)	V_D calc.	LFA calc. (deg)	LFA (deg)	V_D	Wtot	Ψ (rad)
34	14.88020801	0.078541543	4.500098923	14.83483821	0.364576107	0.5777
51	20.55304722	0.157130207	9.002897709	20.78670894	0.570494005	0.3635
67	26.14907779	0.083599502	4.789898647	26.40970725	0.787250151	0.2801
84	32.33458921	0.091692601	5.253599069	32.88205326	0.953021107	0.2515
91	34.91215744	0.091940444	5.267799409	35.18833247	0.949828477	0.2538

Table 15. Free wind velocity 6 m/s

r/R(%)	alfa(deg)	C_L:	Circulation	a'_2	a_2
30	6.656025555	0.605129886	2.760990973	0.017604638	0.069178258
47	9.961850298	0.75434756	4.432415296	-0.004608125	-0.038949598
63	4.992242728	0.714709905	4.789675741	0.010778537	0.221965113
80	5.054593575	0.609377373	4.284849282	0.005066534	0.153817432
95	5.004025591	0.423372842	2.936956796	0.002945329	0.121150995

r/R(%)	V_D calc.	LFA calc. (deg)	LFA (deg)	V_D	Wtot	Ψ (rad)
34	15.16459837	9.003796368	9.0038	15.2221796	0.645610301	0.6695
51	20.76492595	12.41659714	12.4166	21.08072887	0.89708289	0.4482
67	26.27239748	7.438598642	7.4386	26.79526029	1.138316705	0.3557
84	32.41344946	7.373299071	7.3733	33.22811276	1.328287896	0.3195
91	34.97063944	7.110199191	7.1102	35.4475216	1.304728229	0.3233

Table 16. Free wind velocity 8 m/s

r/R(%)	alfa(deg)	C_L:	Circulation	a'_2	a_2
30	14.60969707	1.07165174	5.289114266	0.016666518	0.035521931
47	15.51833606	1.16537299	7.113495082	-0.00598908	-0.028718166
63	8.892858469	0.959872204	6.575876425	0.017304014	0.194973601
80	8.173025418	0.854790139	6.096131168	0.008646487	0.146999192
95	8.067464336	0.605962616	4.247492098	0.004066145	0.091068338

r/R(%)	V_D calc.	LFA calc. (deg)	LFA (deg)	V_D	Wtot	Ψ (rad)
34	16.32177733	18.4814957	18.4815	16.17324242	1.104392367	0.4683
51	21.67856036	18.93509294	18.9351	21.79673057	1.29771348	0.3201
67	27.02081887	12.66749724	12.6675	27.55688854	1.778840828	0.2509
84	33.04281629	11.62659911	11.6266	33.86867079	1.990835367	0.2328
91	35.55464434	11.17349888	11.1735	35.96266948	1.927537751	0.2366

Table 17. Free wind velocity 10 m/s

r/R(%)	alfa(deg)	C_L:	Circulation	a'_2	a_2
30	21.88401105	1.305456645	7.019051106	0.005098604	0.006675704
47	21.29644908	1.315992749	8.402563663	-0.01433056	-0.043026195
63	13.29681042	1.004174817	7.073368773	0.021618048	0.147905316
80	11.79316653	0.997917057	7.246575623	0.010515078	0.109838073
95	11.48710341	0.753601181	5.352401365	0.003365482	0.045926041

r/R(%)	V_D calc.	LFA calc. (deg)	LFA (deg)	V_D	Wtot	Ψ (rad)
34	17.61860759	26.55579111	26.5558	17.37451845	1.463131989	0.4630
51	22.65326903	25.05888939	25.0589	22.68006084	1.513142031	0.3269
67	27.87228417	17.70709806	17.7071	28.29326183	2.149309198	0.2534
84	33.75745398	15.93559774	15.9356	34.58025912	2.440732738	0.2347
91	36.21247193	15.26779667	15.2678	36.48755002	2.388553933	0.2376

Table 18. Free wind velocity 12 m/s

r/R(%)	alfa(deg)	C_L:	Circulation	a'_2	a_2
30	27.77817287	1.422702006	8.355336461	-0.00702973	-0.006247722
47	26.41204619	1.303563115	8.749211025	-0.02295726	-0.047264973
63	17.35298905	1.171916651	8.522839921	0.026003891	0.12018997
80	15.14435743	1.096691192	8.133830222	0.012800498	0.091151161
95	14.362365	0.879289922	6.342591935	0.004253636	0.040100509

r/R(%)	V_D calc.	LFA calc. (deg)	LFA (deg)	V_D	Wtot	Ψ (rad)
34	19.0268422	32.53488849	32.5349	18.50405536	1.647111654	0.4712
51	23.81845261	30.58098639	30.581	23.52194767	1.799001204	0.3294
67	28.85778668	22.07369446	22.0737	28.84571064	2.399298184	0.2563
84	34.60983276	19.78629781	19.7863	35.23309035	2.814916984	0.2361
91	36.99963651	18.75949691	18.7595	37.26184306	2.84488834	0.2377

Table 19. Free wind velocity 14 m/s

r/R(%)	alfa(deg)	C_L:	Circulation	a'_2	a_2
30	32.58871867	1.986917929	12.72619929	-0.017447556	-0.011208646
47	30.930597	0.973094992	6.888567412	-0.031468306	-0.047205925
63	20.85157412	1.185900097	8.930382147	0.03255472	0.109959808
80	18.76948187	0.769160543	5.843936451	0.012131242	0.061420377
95	17.29270099	0.91581661	6.724324233	0.004254639	0.029135726

r/R(%)	V_D calc.	LFA calc. (deg)	LFA (deg)	V_D	Wtot	Ψ (rad)
34	20.67338659	37.83518027	37.8352	19.81622648	2.035501175	0.4664
51	25.02995859	35.00989014	35.0099	24.46440301	1.887294035	0.3450
67	29.91645141	25.69529431	25.6953	29.64515905	2.57356817	0.2675
84	35.43596547	22.86140077	22.8614	36.07935774	2.555881225	0.2529
91	37.8202636	21.62909787	21.6291	37.98778876	2.879137349	0.2483

Table 20. Free wind velocity 16 m/s

r/R(%)	alfa(deg)	C_L:	Circulation	a'_2	a_2
30	37.34711043	1.888924747	13.16493288	-0.047799	-0.022578444
47	35.22531714	0.983114705	7.351792589	-0.044832142	-0.050619243
63	24.65291167	1.204533328	9.422488919	0.034315407	0.086621552
80	21.80883068	0.848223846	6.615776008	0.013934688	0.05367263
95	20.41194372	0.801053117	5.998981913	0.001824877	0.00935406

r/R(%)	V_D calc.	LFA calc. (deg)	LFA (deg)	V_D	Wtot	Ψ (rad)
34	22.32921497	42.48897944	42.489	21.24831912	2.228165881	0.4740
51	26.4424675	39.48749214	39.4875	25.7327003	2.14252889	0.3482
67	31.17381524	29.73769312	29.7377	30.56514204	2.855317038	0.2712
84	36.43364547	25.97519876	25.9752	36.82116352	2.696833308	0.2597
91	38.75509951	24.69590313	24.6959	38.8941851	2.933137942	0.2576

Table 21. Free wind velocity 18 m/s

r/R(%)	alfa(deg)	C_L:	Circulation	a'_2	a_2
30	41.50126948	1.746218644	13.19000427	-0.083671732	-0.02985393
47	38.98745952	1.018796548	8.05467218	-0.057781745	-0.050842956
63	28.10272596	1.205158921	9.810233824	0.036009335	0.070713549
80	24.7066799	0.865245537	6.940935579	0.015556115	0.047090708
95	23.4964889	0.754634114	5.77381589	-0.002162965	-0.008570599

r/R(%)	V_D calc.	LFA calc. (deg)	LFA (deg)	V_D	Wtot	Ψ (rad)
34	24.08930997	46.58807595	46.5881	22.75709923	2.465182257	0.4790
51	27.96178725	43.36628862	43.3663	27.16165461	2.397610253	0.3511
67	32.4878121	33.19658981	33.1966	31.5883695	3.028811214	0.2766
84	37.55201161	29.02609893	29.0261	37.80195355	2.910423599	0.2646
91	39.76957091	27.62169604	27.6217	39.71991967	2.924799545	0.2635

Table 22. Free wind velocity 20 m/s

r/R(%)	alfa(deg)	C_L:	Circulation	a'_2	a_2
30	45.28237625	1.662614545	13.55309208	-0.129029285	-0.035262137
47	42.93602423	1.047510585	8.749357961	-0.084142181	-0.057907875
63	31.18520778	0.980110041	8.312032873	0.038405717	0.060589011
80	27.56679221	0.942817982	7.791304958	0.01581424	0.038437371
95	26.28394284	0.707139697	5.53559761	-0.005370265	-0.017038086

r/R(%)	V_D calc.	LFA calc. (deg)	LFA (deg)	V_D	Wtot	Ψ (rad)
34	25.91870941	50.28957478	50.2896	24.47251702	2.713023453	0.4831
51	29.50903427	47.24508828	47.2451	28.39869275	2.575465488	0.3587
67	33.82650274	36.11108852	36.1111	32.67596408	3.098010719	0.2850
84	38.74755073	31.93939721	31.9394	38.74217087	3.075553286	0.2708
91	40.8587067	30.34469923	30.3447	40.58979469	2.985531	0.2725

Table 23. Free wind velocity 22 m/s

r/R(%)	alfa(deg)	C_L:	Circulation	a'_2	a_2
30	48.48421429	1.524070917	13.35550224	-0.174276581	-0.037249461
47	46.31577573	1.009994569	8.907773503	-0.108507428	-0.059962978
63	34.49010361	0.924811918	8.179081647	0.033808976	0.043083116
80	30.20767145	0.98450212	8.390921273	0.016429797	0.032831743
95	28.90474242	0.689195344	5.526721149	-0.008626869	-0.022427211

r/R(%)	V_D calc.	LFA calc. (deg)	LFA (deg)	V_D	Wtot	Ψ (rad)
34	27.76625378	53.33907239	53.3391	26.42311361	2.918528201	0.4889
51	31.15263748	50.59098706	50.591	30.07027949	2.791405898	0.3633
67	35.34263026	39.43738789	39.4374	34.03554744	3.321169512	0.2895
84	40.04573149	34.67629445	34.6763	39.86496398	3.291538831	0.2746
91	42.07501555	33.04789786	33.0479	41.75684977	3.172838423	0.2768

Table 24. Free wind velocity 24 m/s

r/R(%)	alfa(deg)	C_L:	Circulation	a'_2	a_2
30	51.75466328	1.404866339	13.17201823	-0.240155084	-0.039601507
47	49.62099104	0.97881614	9.101749301	-0.141167983	-0.062976447
63	37.80005393	0.905518318	8.354111742	0.023560827	0.024502631
80	32.68944032	1.033950216	9.096782698	0.01689308	0.028245009
95	31.13870732	0.637760763	5.244647302	-0.009077681	-0.019870234

r/R(%)	V_D calc.	LFA calc. (deg)	LFA (deg)	V_D	Wtot	Ψ (rad)
34	29.65628864	56.45677094	56.4568	28.26105969	3.145536023	0.4933
51	32.8704157	53.86168558	53.8617	31.68033653	3.037535173	0.3660
67	36.96754692	42.78068834	42.7807	35.19955945	3.588252057	0.2921
84	41.42506887	37.23779315	37.2378	40.78353238	3.515932931	0.2777
91	43.35260725	35.35399826	35.354	42.63961005	3.362599635	0.2813

Table 25. Free wind velocity 25 m/s

r/R(%)	alfa(deg)	C_L:	Circulation	a'_2	a_2
30	52.95516265	1.351367595	13.09487505	-0.26225188	-0.038727086
47	50.95349734	0.964295726	9.205666918	-0.152688157	-0.061992894
63	39.22319006	0.903290488	8.510559935	0.020121719	0.019115251
80	33.70236342	1.039571985	9.294331242	0.01938116	0.029991745
95	32.0204505	0.637642751	5.311993553	-0.006871118	-0.013972552

r/R(%)	V_D calc.	LFA calc. (deg)	LFA (deg)	V_D	Wtot	Ψ (rad)
34	30.61736321	57.5933705	57.5934	29.12940694	3.254410904	0.4954
51	33.75424928	55.17648519	55.1765	32.45331592	3.159167979	0.3672
67	37.792389	44.20678829	44.2068	35.80459687	3.715030738	0.2935
84	42.13383515	38.29199302	38.292	41.24779194	3.63177888	0.2789
91	44.02695102	36.31759853	36.3176	43.11546622	3.498401084	0.2824

Appendix C - Aerodynamic 2D Coefficients for S809 Airfoil

Aerodynamic coefficients (α = angle of attack, C_l = lift coefficient, C_{dp} = pressure drag coefficient, C_{dw} = total drag coefficient from wake traverse, C_m = moment coefficient) obtained at the OSU wind tunnel with a Reynolds number from 990,000 to 1,040,000 are shown in table 26.

Table 26 - Wind tunnel profile coefficients from OSU (Re = 1,000,000)

alfa	Cl	Cdp	Cdw	Cm	Re (milj)
-20.1	-0.55	0.2983	0.059	1.01	
-18.2	-0.65	0.2955	0.0797	1.02	
-16.2	-0.8	0.1826	0.0244	1.01	
-14.1	-0.79	0.0793	0.006	0.99	
-12.1	-0.7	0.0547	-0.0043	1.01	
-10.2	-0.63	0.0401	0.075	-0.0035	1
-8.2	-0.58	0.0266	-0.0032	1	
-6.2	-0.61	0.0183	0.0193	0.0088	1
-4.1	-0.4	0.0004	0.0127	-0.0245	0.99
-2.1	-0.16	0.0009	0.009	-0.0308	1
0	0.07	0.0022	0.0085	-0.0356	1.01
2.1	0.3	0.0037	0.0088	-0.0394	1
4.1	0.55	0.005	0.0088	-0.0461	1
6.1	0.79	0.0063	0.009	-0.0499	1
8.2	0.9	0.0096	0.0167	-0.0364	1
10.1	0.94	0.0231	0.0487	-0.0396	1
11.2	0.93	0.0236	-0.028	1	
12.2	0.97	0.0368	-0.0307	1	
13.3	1	0.0551	-0.0362	0.99	
14.2	1.02	0.0618	-0.0365	0.99	
15.2	1.03	0.0705	-0.0375	0.99	
16.2	1.01	0.088	-0.043	1	
17.2	0.95	0.1043	-0.0456	0.99	
18.1	0.9	0.1325	-0.0581	1	
19.2	0.78	0.3474	-0.1464	1.02	
20	0.67	0.3211	-0.1171	1.02	
22.1	0.7	0.3699	-0.1253	1.02	
24	0.77	0.4348	-0.143	1.03	
26.1	0.91	0.5356	-0.1783	1.04	

Aerodynamic coefficients (α = angle of attack, C_l = lift coefficient, C_{dw} = total drag coefficient, C_m = moment coefficient) obtained at the Delft University of Technology (DUT) Low Speed Laboratory low-turbulence wind tunnel with a Reynolds number of 1,000,000 are shown in Table 27.

Table 27 - Wind tunnel profile coefficients from DUT (Re = 1,000,000)

alfa	CL	CD
-1.04	0.019	0.0095
-0.01	0.139	0.0094
1.02	0.258	0.0096
2.05	0.378	0.0099
3.07	0.497	0.01
4.1	0.617	0.01
5.13	0.736	0.0097
6.16	0.851	0.0095
7.18	0.913	0.0127
8.2	0.952	0.0169
9.21	0.973	0.0247
10.2	0.952	0.0375
11.21	0.947	0.0725
12.23	1.007	0.0636
13.22	1.031	0.0703
14.23	1.055	0.0828
15.23	1.062	0.1081
16.22	1.043	0.1425
17.21	0.969	0.1853
18.19	0.938	0.1853
19.18	0.929	0.1853
20.16	0.923	0.1853

Appendix D – SolidBody

Flow Disturbance from a Two-dimensional Solid Body

Björn Montgomerie, Feb. 15, 2004

1. Introduction

The background of the present text is the NREL database from the wind tunnel tests at the NASA Ames, California facility. A 10m diameter wind turbine was tested in the tunnel. One blade was instrumented with pressure holes and pressure probes mounted on the leading edge of the blade at five different radial positions. The tip of each probe had five holes designed to furnish information about the local flow angle and velocity. These probes were meant to help analysts evaluate the angle of attack for the pressure hole sections of the blade.

In an effort to evaluate the aerodynamic coefficients for the blade, the leading edge probe data are reproduced from the known conditions such as the wind speed in the tunnel, the rotational speed of the rotor and last, but not least, the pressure distribution on the blade.

The technique used in this evaluation is to initially conjecture the angle of attack. This allows a conversion from the aerodynamic coefficients for normal and tangential forces (CN and Ct) to the corresponding coefficients for lift and drag (CL and CD). In the next step the circulation on the blade is calculated and then the flow vector, at the probe tip, is calculated and compared with the measured vector. The error is used to guide the algorithm to produce a new angle of attack at the profile and then a new estimate of the probe tip flow vector follows and the iteration continues until a convergence criterion is satisfied.

The algorithm used to calculate the probe tip flow vector uses two modifications to the parallel oncoming flow, the circulation and the deviation of the flow caused by the solid body displacement. The method derived here is the solid body blockage effect in the blade profile section plane.

2. Aerodynamic Fundamentals

Fig. 1 shows the basic aerodynamic element of a point vortex, whose circulation is □. It is located at a point, that can be thought of as a vector *q,* and it effects any point in the xy plane by giving rise to an ”induced” velocity in any such point. *p* is an arbitrary point (position vector) where the induced velocity *v*, caused by the vortex, is evaluated. The Biot-Savart law of induction is used for this purpose. It assumes the following form where □, *p*, *q* and *v* are to be considered vectors in 3D space. The temporary extension to three dimensions is an expedient way to keep track of the induced vector direction.

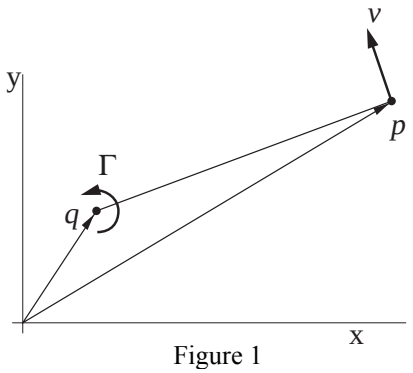

Figure 1

$$v = \frac{1}{2\pi d^2}\Gamma \times (p - q) \qquad (1)$$

Solving the determinant for vector cross multiplication, the resulting vector velocity components become

$$v_x = -\frac{\Gamma}{2\pi d^2}(y_p - y_q) \qquad (2)$$

$$v_y = \frac{\Gamma}{2\pi d^2}(x_p - x_q) \qquad (3)$$

The latter two expressions will be applied in the more complex context below. *q* will be associated with the location of the vortex while *p* will be the point of evaluation of the induced velocity.

3. Application to a Wing Profile

The induction calculation of the previous section is applied in a model of a 2D wing profile by choosing a number of points (q_i) on the circumference of the profile. At these points point vortices are applied. Initially these vortices are unknown as to their circulation strength. By evaluation of the induced velocity, in points mid-way between all q_i, and adding the ambient wind vector in these points a condition that the velocities are aligned with the profile surface leads to an equation system. From this system the unknown circulation strengths can be solved using Gaussian elimination.

4. Equation Foundation

Once the circulations are known their influence anywhere in the plane can be directly calculated. This then applies to the tip of the pressure probe mentioned in the introduction. The induced vector field around this profile will become larger in error the more separated the suction side of the airfoil is.

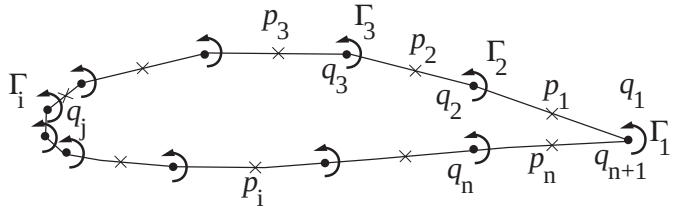

Figure 2

With the model base of Fig. 2 the induced velocity in an arbitrary induction evaluation point *i* is

$$v_{x,i} = -\sum_{i=1}^{n} \frac{\Gamma_j}{2\pi d_{i,j}^2}(y_{p,i} - y_{q,j}) \qquad (4)$$

$$v_{y,i} = \sum_{i=1}^{n} \frac{\Gamma_j}{2\pi d_{i,j}^2}(x_{p,i} - x_{q,j}) \qquad (5)$$

Since the points of induction evaluation are placed mid-way between vortex points, the following expressions can be inserted in (4) and (5).

$$x_{p,i} = \frac{1}{2}\left(x_{q,i} + x_{q,i+1}\right) \qquad (6)$$

$$y_{p,i} = \frac{1}{2}\left(y_{q,i} + y_{q,i+1}\right) \qquad (7)$$

The quantity $d_{i,j}$ is the distance from q_j to p_i. It is obtained from the Pythagorean theorem as follows.

$$d_{i,j} = \sqrt{\left(x_{q,j} - x_{p,i}\right)^2 + \left(y_{q,j} - y_{p,i}\right)^2} \qquad (8)$$

Also the expression (8) need to be inserted in (4) and (5) before summation.

The sum of induction contributions from all vortices, at say p_i, is called v_i. But, also the free stream velocity is superimposed on v_i.

5. Equation Details

From the beginning all vortices are unknown as to their circulation strength. These strengths must be solved from a set of equations that are based on the condition that the induced vector plus the free stream vector be parallel to the surface – or, in fact, an approximation for the surface. Fig. 3 shows one panel of the profile. The induced vector on this panel, together with the free stream vector will be set to be parallel with the line defined by the points q_i and q_{i+1}, although the connection between the two points is generally a curve, not a straight line. This approximation is accepted in this model. It may possibly invite significant errors at the leading edge of the profile because of the high curvature of the surface contour at that location. The cure is to place check points more densely in that region. The flow alignment condition can be formulated as follows.

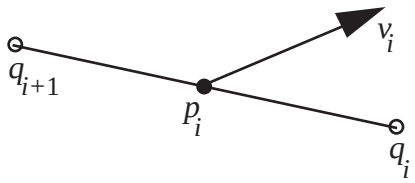

Figure 3

The total velocity, i.e. $V_{\infty,i} + v_i$, at p_i is in alignment with the surface when

$$(V_{\infty,i} + v_i) \times (q_{i+1} - q_i) = 0 \qquad (9)$$

The cross product can be obtained from evaluation of a determinant.

$$\begin{vmatrix} \hat{x} & \hat{y} & \hat{z} \\ V_{\infty,x} + v_{x,i} & V_{\infty,y} + v_{y,i} & 0 \\ x_{q,(i+1)} - x_{q,i} & y_{q,(i+1)} - y_{q,i} & 0 \end{vmatrix} = \begin{Bmatrix} 0 \\ 0 \\ -\left(y_{q,i} - y_{q,i+1}\right)\left(v_{x,i} + V_{\infty,x}\right) + \left(x_{q,i} - x_{q,i+1}\right)\left(v_{y,i} + V_{\infty,y}\right) \end{Bmatrix} \qquad (10)$$

Here $\hat{x}, \hat{y}, \hat{z}$ are unit vectors. Obviously the two-dimensional vectors seen in Fig. 3 have been extended to three dimensions. The result from evaluation of the determinant is thus a vector perpendicular to the surface in Fig. 3. But, this result is only used to be set to zero, which will create the relationships necessary for the set of equations required. Thus from (10), for the surface interval *i,* we have the equation

$$\left(x_{q,i} - x_{q,i+1}\right)\left(v_{y,i} + V_{\infty,y}\right) - \left(y_{q,i} - y_{q,i+1}\right)\left(v_{x,i} + V_{\infty,x}\right) = 0 \qquad (11)$$

In anticipation of later needs this should be written

$$\left(x_{q,i} - x_{q,i+1}\right)v_{y,i} - \left(y_{q,i} - y_{q,i+1}\right)v_{x,i} = -\left(x_{q,i} - x_{q,i+1}\right)V_{\infty,y} + \left(y_{q,i} - y_{q,i+1}\right)V_{\infty,x} \qquad (12)$$

Inserting (4) and (5) in (12) gives for the *i*:th interval, with induction contributions from all vortex points (*j*), the following expression.

$$k_{i1}\Gamma_1 + \ldots + \frac{-\left(y_{p,i} - y_{q,j}\right)\left(y_{q,i+1} - y_{q,i}\right) - \left(x_{p,i} - x_{q,j}\right)\left(x_{q,i+1} - x_{q,i}\right)}{2\pi\left[\left(x_{p,i} - x_{q,j}\right)^2 + \left(y_{p,i} - y_{q,j}\right)^2\right]}\Gamma_j + \ldots\ldots + k_{in}\Gamma_n =$$

$$\left(x_{q,i+1} - x_{q,i}\right)V_{\infty,y} - \left(y_{q,i+1} - y_{q,i}\right)V_{\infty,x} \qquad (13)$$

There are *n* such equations, one for each panel mid-point *i*. Eq. (13) represents a system of equations that can be written as follows.

$$\mathbf{K} \cdot \mathbf{\Gamma} = \mathbf{R} \qquad (14)$$

where

$$\mathbf{K} = \begin{bmatrix} k_{11} & k_{12} & . & k_{1j} & k_{1n} \\ & . & & & \\ & & . & & \\ & & & . & \\ k_{n1} & . & . & . & k_{nn} \end{bmatrix} \quad \text{and} \quad \mathbf{\Gamma} = \begin{Bmatrix} \Gamma_1 \\ \Gamma_2 \\ \ldots \\ \Gamma_j \\ \Gamma_n \end{Bmatrix} \qquad (15)$$

R is also a vector whose typical element is seen as the right member in Eq. (13). Eq. (14) is a straightforward linear system which can be solved for the values using Gauss elimination. The typical k_{ij} element is the busy looking term to the left of the equality sign in Eq. (13).

6. Application

The result from the steps of derivation described above is a set of discrete circulation strengths (Γ) placed as seen in Fig. 2. The strengths are constrained to give a flow that is parallel to the surface of the

profile. But, there is no Kutta condition. The total circulation, i.e. the sum of the individual circulation strengths, turns out not to be zero in the general case. Since the program was generated for the exclusive purpose of providing a body displacement velocity vector, in an arbitrary point outside the airfoil, it should not produce any lift. Therefore no net lift should be generated by the vortices, which means that the sum of circulations should be zero except for insignificant decimal roundings. A method to eliminate the residual lift appears below.

The usefulness of the solution lies in its capability to be used for induction calculation outside of the profile itself. This can be used to estimate the disturbance velocity vector at the position of a probe. Such probes were part of one of the blades on the NREL test wind turbine in the NASA Ames test activity. The analysis of the corresponding test data is in fact the reason for this text. Since the Kutta condition is no part of this analysis, the disturbance, calculated for the probe positions, represents a solid body disturbance without lift effects. The lift effects will have to be provided from other methods. The disturbance can, however, be calculated for any angle of attack. In the application of the program this possibility was utilized.

The equations and the necessary Gaussian elimination, to obtain the □s, were implemented in a Fortran program. The program was used as one of several tools in the analysis of the NREL test data. For reasons to eliminate the residual lift, it turned out to be practical to manipulate the y coordinate of the first point given (yTE), see Fig. 4. By increasing/changing this value, wagging the tail as it were, the net circulation can be decreased/changed until the total circulation becomes zero. The corresponding geometric deformation appears in Fig. 4. The case definition input routine provides the user with a relatively expedient method to accomplish this goal. Zero lift is thus accomplished by running the program several times and setting the yTE parameter to values governed by the learning from the previous iterations. At further utilization of the computer program the search for zero net lift should be implemented as an automatic feature in the code itself.

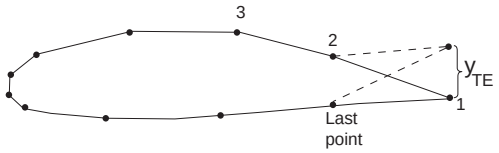

Figure 4

In running the program the point of evaluation, representing the probe position in the NREL tests, was positioned at: x = -0.8 and y = -.1. At a locally felt velocity of 11 m/s, at the 30% chord point, the disturbance velocity at x,y was about 0.2m/s. This disturbance should also be compared to the corresponding lift induced velocities at the same point. The latter were of order of magnitude of 1.5m/s at 8° angle of attack. In summary the displacement disturbance is 13% of the typical lift induced velocity at "normal" operation. The lift induced disturbance was calculated as Biot-Savart induced velocity from a single vortex located at a fraction of chord, which was obtained as Cm/CN. The latter two quantities were directly available from the NREL tests.

Since the method is perfectly inviscid the flow velocity V, which is an input, results in a strength, for the set of vortices, which is directly proportional to V. The induced velocity components (vx,vy) at the point of evaluation (x,y) are also directly proportional to the vortex strength and V. So, by calculating (vx,vy) for a series of angle of attack (□) values, while V was held constant at 10 m/s, a useful database was obtained for all blade profiles that were instrumented in the NREL tests. If e.g. the local velocity were to be say 8 m/s, the (vx,vy) values in the database would be multiplied by 8/10. The database is reproduced below.

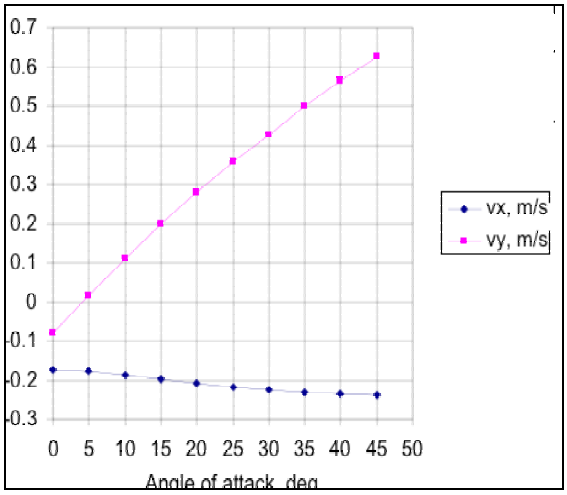

Probe coordinates:

xA =	-0.8	yA =	-0.105
Vlocal =	10	m/s	

alpha	vx, m/s	vy, m/s
0	-0.176	-0.081
5	-0.179	0.016
10	-0.187	0.11
15	-0.198	0.197
20	-0.208	0.28
25	-0.218	0.359
30	-0.225	0.424
35	-0.231	0.499
40	-0.236	0.565
45	-0.238	0.626

Figure 5

7. Accuracy

The simple inviscid flow model described above does not represent the disturbance of the flow field well in case of heavy separation. For such cases the contour of the model should encompass also the separated flow region borders. It was, however, judged that since the correction from the solid blockage is very small, a correction on the correction would not be worth the effort of running additional forms of separated flow representation. The effect was therefore ignored.

Another fact that should be considered is that the method is two-dimensional, i.e. the wing has infinite extent into and out of the plane of the paper (with reference to Fig. 2). Thus, near the tip and the root of the blade the "wing" is only half infinite. Therefore the disturbance velocity should be halved at these positions. In the case of the NREL rotor blade the probe stations were not placed at the very ends of the blade. Perhaps only about 75% of the 2D disturbance should be used for the outboard probe locations. This aberration from the straight-forward application of the solid body disturbance at the probes may turn out to be negligible.